ADVANCED MATERIALS
www.advmat.de

www.MaterialsViews.com

Classification of Lattice Defects in the Kesterite Cu_2ZnSnS_4 and $Cu_2ZnSnSe_4$ Earth-Abundant Solar Cell Absorbers

Shiyou Chen, Aron Walsh, Xin-Gao Gong, and Su-Huai Wei**

The kesterite-structured semiconductors Cu_2ZnSnS_4 and $Cu_2ZnSnSe_4$ are drawing considerable attention recently as the active layers in earth-abundant low-cost thin-film solar cells. The additional number of elements in these quaternary compounds, relative to binary and ternary semiconductors, results in increased flexibility in the material properties. Conversely, a large variety of intrinsic lattice defects can also be formed, which have important influence on their optical and electrical properties, and hence their photovoltaic performance. Experimental identification of these defects is currently limited due to poor sample quality. Here recent theoretical research on defect formation and ionization in kesterite materials is reviewed based on new systematic calculations, and compared with the better studied chalcopyrite materials $CuGaSe_2$ and $CuInSe_2$. Four features are revealed and highlighted: (i) the strong phase-competition between the kesterites and the coexisting secondary compounds; (ii) the intrinsic p-type conductivity determined by the high population of acceptor Cu_{Zn} antisites and Cu vacancies, and their dependence on the Cu/(Zn+Sn) and Zn/Sn ratio; (iii) the role of charge-compensated defect clusters such as $[2Cu_{Zn}+Sn_{Zn}]$, $[V_{Cu}+Zn_{Cu}]$ and $[Zn_{Sn}+2Zn_{Cu}]$ and their contribution to non-stoichiometry; (iv) the electron-trapping effect of the abundant $[2Cu_{Zn}+Sn_{Zn}]$ clusters, especially in Cu_2ZnSnS_4. The calculated properties explain the experimental observation that Cu poor and Zn rich conditions (Cu/(Zn+Sn) ≈ 0.8 and Zn/Sn ≈ 1.2) result in the highest solar cell efficiency, as well as suggesting an efficiency limitation in $Cu_2ZnSn(S,Se)_4$ cells when the S composition is high.

1. Introduction

In the search for low-cost and high-efficiency solar cell absorbers, the semiconductors Cu_2ZnSnS_4 (CZTS) and $Cu_2ZnSnSe_4$ (CZTSe) have drawn intensive attention recently.[1–6] They are expected to be an ideal substitute for the currently commercialized solar cell absorbers CdTe and $Cu(In,Ga)Se_2$ (CIGS). The materials combine: (i) component elements that are earth-abundant and non-toxic; (ii) band gaps (around 1.0 and 1.5 eV,[7–13] respectively) close to the optimal band gaps for single-junction solar cells according to the Shockley-Queisser model;[6,14] (iii) large light absorption coefficients (>10^4 cm^{-1}); (iv) zincblende-derived structures that are related to those of CdTe and CIGS through elemental substitution; (v) electronic structure and optical properties comparable to CIGS, and thus device architectures and growth techniques can be inherited, drawing from decades of research activity.[15]

Studies of Cu_2ZnSnS_4 and $Cu_2ZnSnSe_4$ date back to late 1950s when Goodman and Pamplin designed quaternary I_2-II-IV-VI_4 semiconductors through the cation cross-substitution in I-III-VI_2 chalcopyrites.[16,17] In 1988 Ito and Nakazawa studied the photovoltaic properties of Cu_2ZnSnS_4,[18] and until the late 1990s the solar cell efficiencies were increased to 2.3% by Friedlmeier et al. and to 2.63% by Katagiri et al.[19,20] Since 2005, research on Cu_2ZnSnS_4 and $Cu_2ZnSnSe_4$ based solar cells have drawn an increasing amount of attention, and the efficiency has reached 11.1% recently by Todorov et al. using $Cu_2ZnSn(S,Se)_4$ (CZTSSe) as the absorber layer,[21–23] and 9.2% by Repins et al. for a $Cu_2ZnSnSe_4$ based solar cell.[15] **Table 1** lists the reported CZTS, CZTSe and CZTSSe solar cell performance with efficiencies higher than 5%.

There was a long gap in the time between the first design of quaternary semiconductors and their application in solar cells, and one important reason is that the increased number of component elements make their properties much more complicated than those of binary and ternary semiconductors.[3,24] Lattice defects are important material properties, and are crucial to the application of semiconductors in photovoltaic devices, since they directly influence the generation, separation and recombination of electron-hole pairs. For CZTS and

S. Chen
Key Laboratory of Polar Materials and Devices (MOE)
East China Normal University
Shanghai 200241, China
E-mail: chensy@ee.ecnu.edu.cn
S.-H. Wei
National Renewable Energy Laboratory
Golden, CO 80401, USA
E-mail: suhuai.wei@nrel.gov
S. Chen, X.-G. Gong
Key Laboratory for Computational Physical Sciences (MOE)
Surface Physics Laboratory
Fudan University
Shanghai 200433, China
A. Walsh
Center for Sustainable Chemical Technologies
Department of Chemistry
University of Bath
Claverton Down, Bath BA2 7AY, UK

DOI: 10.1002/adma.201203146

CZTSe, the number of possible lattice defects (e.g. vacancies, interstitials, antisites) increases relative to the well-studied binary and ternary semiconductors. What are the dominant defects in the synthesized samples, and how do they influence their structural, electronic and optical properties? In this perspective review, we show that great progress has been made in answering these questions for the kesterite materials, and we provide a number of new insights into their defect chemistry and physics.

1.1. Observations Related to Defects

Experimentally, there have been scattered reports concerning elemental non-stoichiometry, carrier concentrations, electrical conductivity and other properties of CZTS, CZTSe, and CZTSSe samples, as well as the basic solar cell performance, which are closely related to the intrinsic lattice defects.

(1) Non-stoichiometry: The stoichiometric ratio of Cu, Zn, Sn and S (or Se) elements is 2:1:1:4, i.e., Cu/(Zn+Sn) = 1, Zn/Sn = 1 and (Cu+Zn+Sn)/S = 1; however, most of the CZTS and CZTSe samples synthesized so far are non-stoichiometric, and these ratios deviate from the integral values. In **Figure 1**, the distribution of Cu/(Zn+Sn) and Zn/Sn ratios for the reported solar cells with different efficiencies are plotted. Obviously, most of the solar cells have Cu/(Zn+Sn) ratio between 0.75 and 1, and Zn/Sn ratio between 1 and 1.25, with deviation by as large as 30%. All the cells with efficiencies higher than 8% have these two ratios around 0.8 and 1.2, respectively. This is mentioned frequently as an empirical rule that the Cu poor and Zn rich growth condition gives the highest solar cell efficiency;[1,3,5,6,15,25–29] however, the underlying mechanism is not clear.

Two possible reasons are responsible for the significant non-stoichiometry in CZTS and CZTSe samples, the coexistence of the secondary phases and the high concentration of intrinsic defects or defect clusters. CZTS or CZTSe has a series of competitive binary and ternary compounds, e.g. for CZTS these include CuS, Cu_2S, ZnS, SnS, SnS_2, Cu_2SnS_3, etc. which may form as the secondary phases depending on the synthesis conditions.[30–33] Furthermore, Cu_2ZnSnS_4 (similarly for $Cu_2ZnSnSe_4$) can be synthesized using these compounds (Cu_2S+ZnS+SnS_2, 2CuS+ZnS+SnS or Cu_2SnS_3+ZnS) as the starting materials,[30,31,34–40] therefore their coexistence is highly possible. The detection of the secondary phases has been given much attention recently.[4,11,15,28,31,41–43] Some compounds such as CuS, Cu_2S, SnS, and SnS_2 have totally different crystal structures from CZTS and are detectable according to the X-ray diffraction (XRD) patterns; however, the structures of ZnS and Cu_2SnS_3 have the same zincblende framework as CZTS,[44] and they are difficult to be detected using XRD techniques alone. Alternative techniques such as energy-dispersive X-ray spectroscopy (EDS),[45] Raman scattering analysis,[46–48] and X-ray absorption near edge structure analysis,[49] have been used to identify the ZnS, Cu-Sn-S, ZnSe, Cu-Sn-Se related secondary phases. Direct evidence of the coexistence of ZnS and ZnSe near the CZTS/Mo and CZTSe/Mo interfaces, and sometimes even in the CZTS samples with the ideal Zn/Sn ratio,[49,50] have been reported.

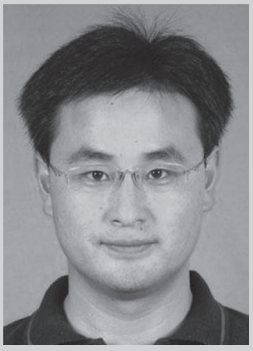

Shiyou Chen is an Associate Professor in the Department of Electronic Engineering and the Key Laboratory for Polar Materials and Devices (MOE), East China Normal University. He obtained his PhD in Condensed Matter Physics from Fudan University in 2009. His research focuses on the calculation of multicomponent semiconductors for photovoltaic and photocatalytic applications.

Aron Walsh is a Reader in Chemistry and a Royal Society University Research Fellow at the University of Bath. He obtained his PhD in Computational Chemistry from Trinity College Dublin in 2006 and has since worked at the National Renewable Energy Laboratory and University College London. His research focuses on the development and application of modelling techniques for functional materials design and characterisation.

Xin-Gao Gong received his PhD from the Institute of Solid State Physics, Chinese Academy of Sciences, in 1993. He joined Fudan University in 2000 and is currently a Xie Xide Chair Professor of Physics, and also Director of the Key Laboratory of Computational Physical Sciences, Ministry of Education. His research is focused on computational studies of the structural and electronic properties of materials. He is a fellow of the American Physical Society.

Su-Huai Wei received his PhD from the College of William and Mary in 1985. He joined the National Renewable Energy Laboratory in 1985 and is currently a Principal Scientist and Manager for the Theoretical Materials Science Group. His research is focused on developing electronic structure theory of materials, especially for energy applications. He is a Fellow of the American Physical Society.

Table 1. The reported performance parameters (open circuit voltage V_{oc}, short circuit current density J_{sc}, fill factor (FF) and light-to-electricity conversion efficiency η) of Cu_2ZnSnS_4, $Cu_2ZnSnSe_4$ and $Cu_2ZnSn(S,Se)_4$ based solar cells with variable chemical components as described by the Cu/(Zn+Sn) and Zn/Sn ratios.

Component	Cu/(Zn+Sn)	Zn/Sn	V_{oc} (mV)	J_{sc} (mA/cm^2)	FF (%)	η (%)	References
Cu_2ZnSnS_4	0.85	1.25	610	17.9	62	6.77	[72]
Cu_2ZnSnS_4	0.82	1.2	587	17.8	65	6.81	[65]
Cu_2ZnSnS_4	~0.78	~1.25	661	19.5	65.8	8.4	[28]
$Cu_2ZnSnSe_4$	0.86	1.15	377	37.4	64.9	9.15	[15]
$Cu_2ZnSn(S,Se)_4$	0.925	1.0	622	15.87	60	5.9	[12]
$Cu_2ZnSn(S,Se)_4$	0.79	1.11	420	30.4	52.7	7.2	[82]
$Cu_2ZnSn(S,Se)_4$	0.9	1.1	497	20		5.4	[83]
$Cu_2ZnSn(S,Se)_4$	0.8	1.22	562.7	24.07	60	8.13	[84]
$Cu_2ZnSn(S,Se)_4$	0.8	1.2	516	28.6	65	9.66	[1]
$Cu_2ZnSn(S,Se)_4$	0.8	1.2	517	30.8	63.7	10.1	[22]
$Cu_2ZnSn(S,Se)_4$			459.8	34.5	69.8	11.1	[21]

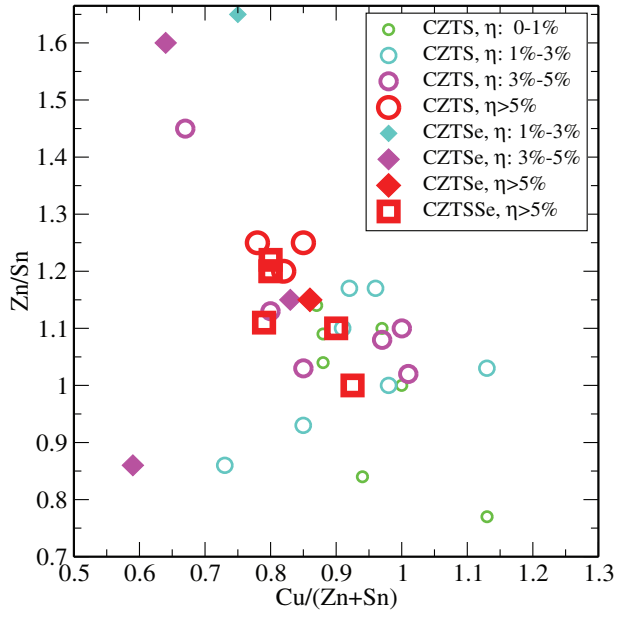

Figure 1. The element ratio (Cu/(Zn+Sn) and Zn/Sn) distribution of the Cu_2ZnSnS_4, $Cu_2ZnSnSe_4$ and $Cu_2ZnSn(S,Se)_4$ based solar cells with different light to electricity conversion efficiencies.[1,6,12,15,22,27–29,35,65,67,72–84]

For the samples without secondary phases, non-stoichiometry results mainly from the high population of intrinsic defects. Possible defects include the Cu, Zn, Sn or S vacancies (V_{Cu}, V_{Zn}, V_{Sn} and V_S), interstitials (Cu_i, Zn_i, Sn_i and S_i), and the antisites A_B with element A replacing element B (Cu_{Zn}, Zn_{Cu}, Zn_{Sn}, Sn_{Zn}, etc.). Besides these, the donor and acceptor defects may also compensate and attract each other, forming defect clusters (V_{Cu}+Zn_{Cu}, $2Cu_{Zn}$+Sn_{Zn}, Zn_{Sn}+$2Zn_{Cu}$). In ternary $CuInSe_2$, $2V_{Cu}$+In_{Cu} defect clusters with very high populations can give rise to a significantly lower Cu/In ratio than unity, e.g. the non-stoichiometric phases $CuIn_5Se_8$ and $CuIn_3Se_5$ have been synthesized.[51–54] Similarly, the high population of defect clusters in CZTS and CZTSe samples can also cause serious non-stoichiometry. However, it is currently a question of what kind of intrinsic defects are dominant in the samples with different Cu/(Zn+Sn) and Zn/Sn ratios.

(2) *Carrier concentrations:* The ionization of intrinsic acceptor and donor defects produces holes and electrons, respectively, so the high population of intrinsic defects can cause high carrier concentrations in the samples and thus influence the electrical conductivity. CZTS, CZTSe and CZTSSe samples have been widely found to show the p-type (hole mediated) conductivity intrinsically,[8,20,34,37,55–64] while n-type samples have not been reported. Despite the certainty of the p-type character, the reported concentration of the majority carriers (holes) from different experiments varies significantly, spanning a range from 1.2×10^{15} to 3.1×10^{20} cm^{-3}, as shown in References.[22,32,34,56,64–71]

Three factors may contribute to the significant scatter in the numbers, including the uncertainties of different measurement techniques,[64–67,69,70] the influence of secondary phases (e.g., the p-type $Cu_{2-x}Se$ secondary phase can contribute in CZTSe samples[41,42]), and the component difference quantified by the deviation of Cu/(Zn+Sn) and Zn/Sn ratios from unity. Considering the large difference in the Cu/(Zn+Sn) and Zn/Sn ratios, the third contribution can be very large. If we assume Cu vacancy (V_{Cu}) and Zn_{Sn} antisite defects cause the deviation of Cu/(Zn+Sn) and Zn/Sn ratios, respectively, a simple estimate shows that a 1% deviation requires the concentration of V_{Cu} and Zn_{Sn} defects to be as high as 10^{20} cm^{-3}, which will generate holes with the same order of concentration provided they are completely ionized. If this assumption is true, the hole concentration would increase linearly with 1-Cu/(Zn+Sn) and Zn/Sn-1 and can be as large as 5×10^{21} cm^{-3} when 1-Cu/(Zn+Sn) = 0.2 and Zn/Sn-1 = 0.2. However, the real situation is much more complicated, because the defect clusters such as V_{Cu}+Zn_{Cu} and Zn_{Sn}+$2Zn_{Cu}$ can also be formed and contribute to the Cu/(Zn+Sn) and Zn/Sn deviations. Such defect clusters are charge-neutral, without any contribution to the carrier concentrations,

so the concentration of holes can be still low even when the Cu/(Zn+Sn) and Zn/Sn deviation is large.

Although plenty of papers have reported the synthesis of CZTS, CZTSe and CZTSSe samples with different stoichiometric ratios, the relationship between the hole concentration and the element ratios is so far not clear, e.g., it is unknown why the hole concentration is even lower in the samples with Cu/(Zn+Sn)≈0.8 (at the order 10^{15} cm^{-3} [22,65]) than in those with value closer to 1 (10^{18} cm^{-3} [32,56]). On the other hand, considering that a low Cu/(Zn+Sn) ratio around 0.8 is reported to be crucial for high solar cell efficiency, one can arrive at the conclusion that the high efficiency is achieved at relatively low concentration of the majority carrier, rather than a high concentration. This seems difficult to understand because it is usually expected that a relatively high carrier concentration should be beneficial for the electrical conductivity and thus the solar cell performance. These open questions limit the optimization of solar cell performance through tuning of the electrical conductivity of the absorber layer.

(3) V_{oc}, J_{sc} and FF: Besides the scatter in the levels of non-stoichiometry and carrier concentrations, the device performance parameters (open circuit voltage, V_{oc}; short circuit current, J_{sc}; and fill factor, FF) reported by different groups are also scattered.[1,6,12,15,22,27–29,35,65,67,72–84] V_{oc} of most CZTS cells span a range from 350 to 650 mV, but their J_{sc} are generally low, spanning a range from 3 to 20 mA/cm^2; V_{oc} of CZTSe cells are generally low, at about 200 to 400 mV, but their J_{sc} span a range from 20 to 40 mA/cm^2. CZTSSe cells combine the higher V_{oc} from CZTS and the higher J_{sc} from CZTSe and are thus usually higher in the overall efficiency, as reported in several recent experiments about CZTSSe cells with low S composition.[1,6,12,23,82]

Understanding what factors in the fundamental properties of absorber semiconductors limit V_{oc}, J_{sc}, FF and the resultant efficiency has become an urgent problem that needs to be addressed in this field, e.g., Barkhouse et al. proposed that their record CZTSSe device is primarily limited by the interface recombination, minority carrier lifetime and series resistance.[22] Obviously intrinsic defects in the CZTS, CZTSe and CZTSSe lattices are an important factor and can have a significant influence on these issues, either directly or indirectly. The deep defect levels can not only diminish J_{sc} through acting as recombination centers for electron-hole pairs and decreasing the minority carrier lifetime, but also limit the V_{oc}. On the other hand, intrinsic defects are also responsible for the self-doping of a semiconductor (influencing the carrier concentration), and can influence the electrical conductivity, the serial resistance, and thus both FF and V_{oc}. Therefore a comprehensive understanding of different intrinsic defects is crucial for investigating these limiting factors. Furthermore, it may reveal the relationship between the element ratios [Cu/(Zn+Sn) and Zn/Sn], the defects, the electrical and optical properties, and the solar cell performance.

1.2. Challenges in the Study of Defects

Although there are various methods to measure the element ratios, the carrier type and concentration, and the device performance, it remains a challenge to study the isolated defects or defect clusters in the synthesized samples. Such studies require high quality crystal samples, which are rare for the quaternary CZTS and CZTSe compounds. Optical (e.g., photoluminescence or deep-level transient spectroscopy[10,61,66,85,86]) and other (capacitance and admittance spectroscopy[22,87,88]) techniques can give important information on the defect transition (activation, ionization) energy levels in the band gap and even the defect or carrier concentration, but it still requires speculation on the origin of those levels as well as what are the dominant defects in the samples. Currently, experimental studies are more abundant on the thin-film synthesis and device fabrication (Table 1) as well as the nanocrystal synthesis,[82,89–93] but limited work has been done to reveal the fundamental factors associated with the intrinsic defects.

A state-of-the-art first-principles approach based on density functional theory (DFT) offers an alternative method for avoiding the difficulty in the experimental methods. Calculations based on DFT can give a direct microscopic picture of the formation and ionization of individual defects and are hence highly complementary to experimental studies. Efficient calculation models have been developed and widely used to investigate the defects in various classes of semiconductors, including not only the group IV, III-V, II-VI semiconductors with the common zincblende and wurtzite structures, but also many new semiconductors (such as metal oxides) with more complicated structures.[94–96] It has also been used in studying the defects in the chalcopyrite and kesterite semiconductors recently,[51,52,97–103] which will be reviewed here.

In the following, the theoretical study of the defect properties will be reported in the order:

(i) defect simulation methods;
(ii) phase stability of $CuInSe_2$, $CuGaSe_2$, Cu_2ZnSnS_4 and $Cu_2ZnSnSe_4$ relative to their secondary phases;
(iii) defect formation and ionization in $CuInSe_2$ and $CuGaSe_2$;
(iv) defect formation and ionization in Cu_2ZnSnS_4 and $Cu_2ZnSnSe_4$;
(v) defect and carrier concentration control in Cu_2ZnSnS_4 and $Cu_2ZnSnSe_4$.

2. Defect Simulation Methods

2.1. Equilibrium Defect Concentrations

The probability of the formation of an intrinsic defect is determined by its energy of formation. For a point defect α in the charge state q, its equilibrium concentration in a crystal can be given by,

$$c(\alpha, q) = N_{sites} g_q e^{\frac{-\Delta H(\alpha,q)}{k_B T}} \quad (1)$$

where k_B is the Boltzmann constant, T is the temperature, $\Delta H(\alpha, q)$ is the formation energy (the vibrational entropy contribution is neglected), N_{sites} is the number of possible atomic sites at which the defect may be formed. g_q is the degeneracy factor, which equals the number of possible configurations for electrons occupying the defect levels and changes with the

charge state q.[104,105] This relation is true at thermodynamic equilibrium and in the dilute regime where the concentration is sufficiently low that defect-defect interactions are negligible. With the information about the formation energies of different defects, the transition energy levels between charge states, the crystal structure, and electronic band gap and effective masses, the defect and carrier concentration and the Fermi energy can be calculated self-consistently, as discussed by Ma et al. in Ref. [105] for CdTe.

2.2. Supercell Model

To simulate the formation of point defects in semiconductors, the supercell model has been developed and widely used, in which a defect is placed in a large supercell, e.g., with 64, 128, 256 or 512 atoms, assuming that the interaction with the image defects in the neighboring cells are negligible. Through the standard first-principles total energy calculation, the defect formation energy $\Delta H(\alpha)$ can be derived according to,

$$\Delta H(\alpha) = E(\alpha) - E(host) + \sum_i n_i(E_i + \mu_i) \quad (2)$$

where $E(host)$ and $E(\alpha)$ is the total energy of the supercell without and with a defect α, respectively. E_i is the total energy of the component element i in its pure phase, e.g., Cu and Zn metals with the FCC structure, Sn crystal with α-Sn structure, Ga and In with the Ga (III) structure (space group I4/mmm), α-S (S_8), and Se with the monoclinic α-Se structure in the present study; n_i is the number of atoms i removed from the supercell to the external reservoir of the element i with the chemical potential μ_i in forming the defect α, e.g., $n_{Cu} = -1$ and $n_{Zn} = 1$ for $\alpha = Cu_{Zn}$. μ_i is referenced to the total energy E_i of the pure element phase, and $\mu_i = 0$ means the element is so rich that the pure element phase can form. From this formulation, it is clear that the formation energy of a defect is a function of the elemental chemical potentials (i.e. growth or annealing environment).

For the ionized defect α in the charge state q, its formation energy $\Delta H(\alpha, q)$ is also a function of the electron chemical potential represented by the Fermi energy E_F,

$$\Delta H(\alpha, q) = E(\alpha, q) - E(host) + \sum_i n_i(E_i + \mu_i) + q\,[\varepsilon_{VBM}(host) + E_F] \quad (3)$$

where $E(\alpha, q)$ is the total energy of the supercell with a defect α in the charge state q, and E_F is relative to the valence band maximum (VBM) of the host $\varepsilon_{VBM}(host)$. For non-degenerate semiconductors valid values of E_F range from the VBM to the conduction band minimum (CBM), i.e., from 0 to the value of the band gap. In a periodic supercell, an absolute reference potential is ill-defined, and the calculated eigenvalue spectra from different calculations are not directly comparable, so a common reference (the deep 1s core levels of the atoms far away from the defects) is used in our approach.

For a given value of E_F, the defect is stable at the charge state with the lowest formation energy amongst all the accessible charge states. The defect transition energy level $\varepsilon_\alpha(q/q')$ is defined as the E_F at which the formation energy $\Delta H(\alpha, q)$ of the α defect with a charge q is equal to $\Delta H(\alpha, q')$ with a different charge q'. This represents the adiabatic (thermal) transition energy between two defect charge states, which includes effects relating to structural relaxation.[51,94]

More calculation details are given in Ref. [98], and the improvement in the current work includes: (i) a larger 128-atom supercell is used as standard, (ii) both the valence band overestimation and conduction band underestimation (Δ_{VBM} = 0.40, 0.39, 0.36 and 0.36 eV, Δ_{CBM} = 1.01, 0.92, 1.30 and 1.04 eV for CZTS, CZTSe, CGSe and CISe in order) are corrected using the same procedure as given for CGSe and CISe in Ref. [52,120], (iii) for donor defects with deep levels (Sn_{Cu}, Sn_{Zn}, Zn_i), Δ_{CBM} is corrected partially according to the dispersion of the corresponding defect band, which gives results more consistent with those from calculations using a non-local hybrid density functional.[100,124]

3. Chemical Potential Range

3.1. Secondary Phase Competition

Under different growth conditions, e.g. elemental partial pressures, the populations of various intrinsic defects are also different, which can be quantitatively described by their formation energy dependence on the chemical potentials, as given by Equation 3. To study the defect properties, the possible chemical potential range of the component elements that favors the growth of the target compound semiconductors ($CuInSe_2$, $CuGaSe_2$, Cu_2ZnSnS_4 and $Cu_2ZnSnSe_4$) should be determined first. A series of thermodynamic conditions must be satisfied: (i) the sum of the chemical potentials of the component elements should be at the equilibrium with the formation energy of the compounds, e.g., the following equations for $CuInSe_2$ and $Cu_2ZnSnSe_4$:

$$\begin{aligned} \mu_{Cu} + \mu_{In} + 2\mu_{Se} &= \Delta H_f(CuInSe_2) \\ 2\mu_{Cu} + \mu_{Zn} + \mu_{Sn} + 4\mu_{Se} &= \Delta H_f(Cu_2ZnSnSe_4) \end{aligned} \quad (4)$$

where $\Delta H_f(X)$ relates to the formation energy of the compound X (the energy change during the formation of the compound from the pure phases of the component elements, $\Delta H_f(CuInSe_2)$ = –1.86 eV and $\Delta H_f(Cu_2ZnSnSe_4)$ = –3.31 eV). (ii) The formation of the secondary compounds, such as CuSe, Cu_2Se, InSe, and $CuIn_5Se_8$ for $CuInSe_2$, and CuSe, Cu_2Se, ZnSe, SnSe, $SnSe_2$ and Cu_2SnSe_3 for $Cu_2ZnSnSe_4$, should be avoided, as described by the following relations:

$$\begin{aligned} \mu_{Cu} + \mu_{Se} &< \Delta H_f(CuSe) = -0.30\,eV \\ 2\mu_{Cu} + \mu_{Se} &< \Delta H_f(Cu_2Se) = -0.24\,eV \\ \mu_{In} + \mu_{Se} &< \Delta H_f(InSe) = -1.09\,eV \\ \mu_{Cu} + 5\mu_{In} + 8\mu_{Se} &< \Delta H_f(CuIn_5Se_8) = -7.28\,eV \\ \mu_{Zn} + \mu_{Se} &< \Delta H_f(ZnSe) = -1.45\,eV \\ \mu_{Sn} + \mu_{Se} &< \Delta H_f(SnSe) = -0.90\,eV \\ \mu_{Sn} + 2\mu_{Se} &< \Delta H_f(SnSe_2) = -1.04\,eV \\ 2\mu_{Cu} + \mu_{Sn} + 3\mu_{Se} &< \Delta H_f(Cu_2SnSe_3) = -1.80\,eV \end{aligned} \quad (5)$$

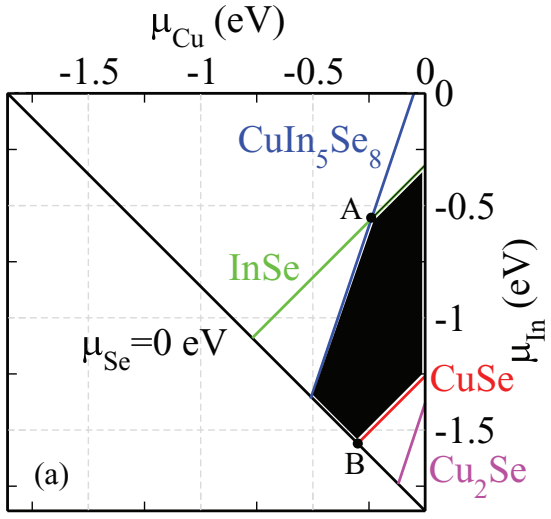

Figure 2. The calculated stable chemical potential region of $CuInSe_2$ in the (μ_{Cu}, μ_{In}) plane. The black area shows the chemical potentials under which $CuInSe_2$ is thermodynamically stable against different competing secondary compounds (represented by the lines with the corresponding colors).

In principle, all of the possible secondary compounds should be considered, while the limit is usually determined by the stable ones that have been well studied. (iii) All of the component elements should favor the formation of the compound, rather than the pure elemental phase, thus, $\mu_{Cu} < 0$, $\mu_{Zn} < 0$, $\mu_{In} < 0$, $\mu_{Sn} < 0$, and $\mu_{Se} < 0$. When the elemental chemical potentials satisfy all the above conditions, the single-phase $CuInSe_2$ and $Cu_2ZnSnSe_4$ compounds should be stable thermodynamically without the coexistence of any secondary phases.

3.2. Stable Chemical Potential Range

With the thermodynamic conditions established, now we can discuss the chemical potential limits for the ternary and quaternary compounds. For $CuInSe_2$, only two of the chemical potentials μ_{Cu}, μ_{In} and μ_{Se} are independent as a result of Equation 4. If μ_{Cu} and μ_{In} are chosen as the variables, their allowed range limited by the above inequalities can be plotted in a 2-dimensional (μ_{Cu}, μ_{In}) plane, as shown in **Figure 2**. $\mu_{Cu} < 0$, $\mu_{In} < 0$ and $\mu_{Se} < 0$ limit the range in the triangle and the inequalities (5) further limit it in the black region, i.e., beyond the green (blue, red) line the formation of InSe ($CuIn_5Se_8$, CuSe) becomes possible. A similar chemical potential region exists for $CuGaSe_2$.

For the quaternary compound $Cu_2ZnSnSe_4$, the limit to the chemical potential region is more complicated. As a result of Equation 4, μ_{Cu}, μ_{Zn} and μ_{Sn} can be independent variables. The stable region limited by the inequalities (5) is bound in a polyhedron in the 3-dimensional (μ_{Cu}, μ_{Zn}, μ_{Sn}) space. To show the region more clearly, two planes with $\mu_{Cu} = -0.20$ and –0.40 eV are plotted in **Figure 3** (right column), in which the triangle determined by $\mu_{Zn} < 0$, $\mu_{Sn} < 0$ and $\mu_{Se} < 0$ becomes smaller when μ_{Cu} becomes more negative. The stable region of $Cu_2ZnSnSe_4$ against CuSe, Cu_2Se, ZnSe, SnSe, $SnSe_2$ and Cu_2SnSe_3 is very narrow as shown by the black area, and it becomes only a point in the $\mu_{Cu} = -0.40$ eV plane. This indicates the range of μ_{Cu} that stabilizes single-phase $Cu_2ZnSnSe_4$ is between –0.40 and 0 eV, and Cu cannot be poorer than the condition under which $\mu_{Cu} =$ –0.40 eV. Similarly the chemical potential range that stabilizes Cu_2ZnSnS_4 against CuS, Cu_2S, ZnS, SnS, SnS_2 and Cu_2SnS_3 is also plotted in Figure 3 (left column). Comparing the stable regions of CZTS and CZTSe, we can see that the shapes are similar because they are limited by similar secondary compounds (binary and ternary sulfides and selenides).

The strictest limit comes from ZnS (ZnSe) and Cu_2SnS_3 (Cu_2SnSe_3), which will form spontaneously when Zn is too rich or too poor, respectively. The resultant Zn chemical potential μ_{Zn} lies in an extremely narrow range (less than 0.2 eV), thus making its control crucial for synthesizing stoichiometric single-crystals. Relatively speaking, the range of stable μ_{Cu}, μ_{Sn} and μ_{Se} are wider (more than 0.4 eV).

Compared with the stable region of $CuInSe_2$, the μ_{Cu} range (between –0.4 and 0 eV) of $Cu_2ZnSnSe_4$ is slightly narrower than that of $CuInSe_2$ (between -0.5 and 0 eV); however, the μ_{Zn} range (about 0.2 eV wide) and μ_{Sn} range (about 0.6 eV wide) are much narrower than that of μ_{In} (about 1.0 eV). $Cu_2ZnSnSe_4$ can be taken as being derived from $CuInSe_2$ through replacing two In by Zn and Sn, which makes the crystal structure satisfy the local charge-neutrality (octet) condition,[24,106] but this analysis shows that more strict chemical potential control of the two cations Zn and Sn is necessary in the synthesis of the derived quaternary compounds.

Phase inhomogeneity is frequently observed in synthesized CZTS and CZTSe samples,[4,11,41,45,46,49,107,108] which is natural considering their narrow stable chemical potential range. This highlights the necessity of careful analysis of the component uniformity in experimental synthesis of the quaternary semiconductors, i.e., excluding the coexistence of binary and ternary secondary compounds, especially for the samples with serious non-stoichiometry Cu/(Zn+Sn) = 0.8 and Zn/Sn = 1.2. Some phases (ZnS and Cu_2SnS_3) are difficult to distinguish due to the structural similarity.[46,47,49] Only when the component uniformity (no secondary phases coexist) is guaranteed, can the non-stoichiometry as shown in Table 1 be taken as being caused by the intrinsic defects, and the electrical and optical properties of the samples can be explained based on the point defect properties.

4. Defect Formation and Ionization in Chalcopyrites

Now we will introduce briefly the defect properties of the ternary chalcopyrites. More specific discussion can be found in Ref. [51,52,103,109–114]. The defect formation energy change as a function of the Fermi energy is plotted in **Figure 4** for six possible defects in $CuInSe_2$ and $CuGaSe_2$, under the chemical potential condition that Cu is so poor that $CuIn_5Se_8$ or $CuGa_5Se_8$ can be formed, as shown by the point A in Figure 2. For a given Fermi energy, only the most stable charge state is plotted, and the charge state changes at the circles (open for acceptors and filled for donors), which correspond to transition energy levels within the bandgap of a material. From Figure 4, we can observe three important characteristics:

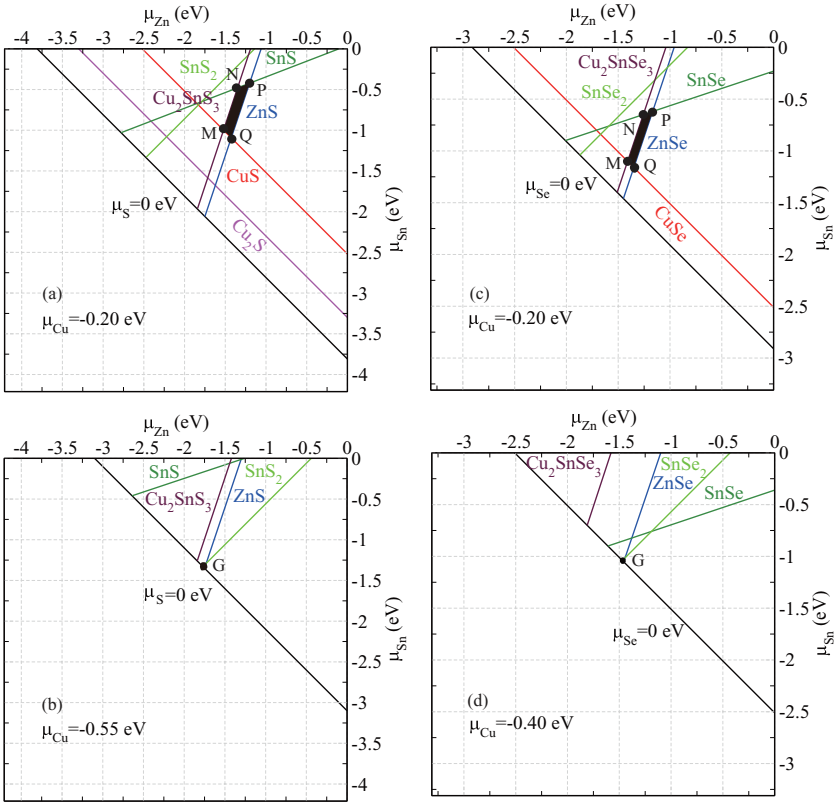

Figure 3. The calculated stable chemical potential region (black area) of Cu_2ZnSnS_4 (left)[97,98] and $Cu_2ZnSnSe_4$ (right) in (μ_{Zn}, μ_{Sn}) planes with different μ_{Cu} in the (μ_{Cu}, μ_{Zn}, μ_{Sn}) chemical potential spaces.

(1) The V_{Cu} acceptor has a shallow transition (ionization) energy level and much lower formation energy than the donor defects like In_{Cu} (Ga_{Cu}) and Cu_i, which explains the intrinsic p-type conductivity and the difficulty to dope $CuInSe_2$ and $CuGaSe_2$ to n-type.[51,52,109,114] Other acceptors such as Cu_{In} and V_{In} have much deeper levels and high formation energies under the Cu poor conditions, so their effect can be neglected, but under Cu rich conditions, their formation can be favored and diminish the solar cell performance.[113]

(2) The In_{Cu} or Ga_{Cu} antisites have relatively deeper donor levels than Cu_i, and especially the Ga_{Cu} levels are quite deep and have been reported to form electron-traps as DX centers.[103, 109, 113] The deeper Ga_{Cu} and In_{Cu} donor levels can be understood based on the low Ga 4s and In 5s orbital energies.[24] In p-type samples with Fermi energy close to VBM, the formation energy of the ionized Ga_{Cu}^{2+} is reduced to a low value (Figure 4), and can be further decreased if Cu becomes poorer, which can be detrimental to solar cell performance. The much deeper Ga_{Cu} levels than In_{Cu} are considered as one important reason for limiting the photovoltaic performance of $CuIn_{1-x}Ga_xSe_2$ alloys with high Ga composition.[109,115]

(3) Donor-acceptor compensation between V_{Cu} and In_{Cu} (In_{Cu}) is energetically favored and popular in the ternary chalcopyrites, leading to facile formation of $2V_{Cu}+In_{Cu}$ ($2V_{Cu}+In_{Cu}$) defect clusters and even the formation of the ordered vacancy compounds (OVC) such as $CuIn_5Se_8$.[51–54] When the acceptor and donor defects aggregate, the formation energy of the defect cluster can be significantly lowered relative to the sum of the isolated defects, contributed by three factors: (i) Charge compensation, i.e., the electrons which occupy the high-energy donor states will transfer to the acceptor site and occupy the low-energy acceptor state, making both the donor and acceptor charged. The energy lowering due to this compensation could be as large as the band gap; (ii) Coulomb attraction between the charged donors and acceptors; (iii) Strain relief.[51,98] For example, when V_{Cu} and In_{Cu} aggregate, the resultant $[2V_{Cu}^{-}+In_{Cu}^{2+}]$ defect cluster has a formation energy of less than 0.1 eV (see Figure 4).

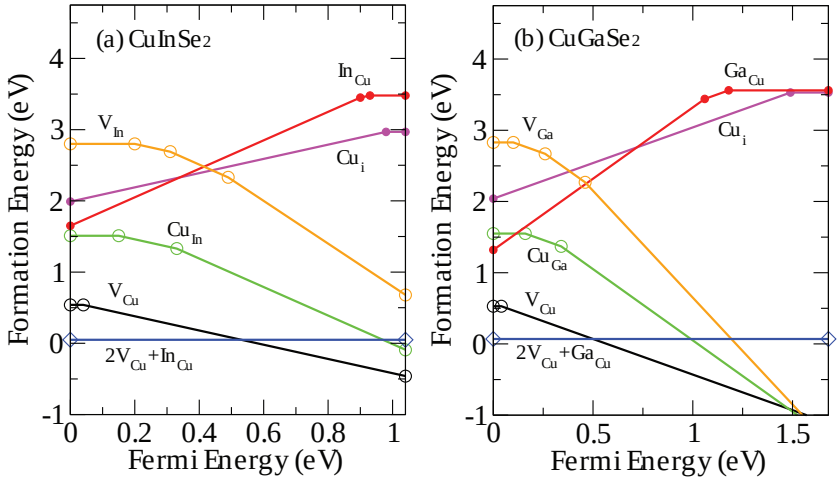

Figure 4. The change of the defect formation energy in $CuInSe_2$ (a) and $CuGaSe_2$ (b) as a function of the Fermi energy, under the elemental chemical potential conditions (point A as shown in Figure 2).

The positive effect of the donor-acceptor compensation is that the deep donor level of In_{Cu} is removed from the gap for the isolated $2V_{Cu}+In_{Cu}$ cluster, and there is even a type-II band alignment between the Cu-poor OVC (like $CuIn_5Se_8$) and stoichiometric $CuInSe_2$.[116] This is considered as a reason for the good photovoltaic performance of non-stoichiometric $CuIn_{1-x}Ga_xSe_2$ solar cells, because the grain-boundaries are usually Cu poor,[117] and the type-II alignment between the Cu poor and rich regions can facilitate the separation of the photo-generated electron-hole pairs.[118] However, when the Ga composition is high, the positive effect becomes limited, which can be explained according to: (i) in $CuGaSe_2$ the compensation of $2V_{Cu}+Ga_{Cu}$

can not fully remove the deep Ga_{Cu} level from the gap due to the too low Ga 4s orbital energy, and (ii) the OVC has a low conduction band, limiting the band gap increase obtainable through increasing the Ga composition. This is another possible reason for the degraded performance of $CuIn_{1-x}Ga_xSe_2$ solar cells with high Ga composition.

5. Defect Formation and Ionization in Kesterites

5.1. Electron Acceptors and Donors

Compared to the ternary chalcopyrites, Cu_2ZnSnS_4 and $Cu_2ZnSnSe_4$ have more intrinsic defects, including V_{Cu}, V_{Zn}, V_{Sn} and V_{Se} vacancies, Cu_{Zn}, Zn_{Cu}, Cu_{Sn}, Sn_{Cu}, Zn_{Sn} and Sn_{Zn} antisites, Cu_i, Zn_i, Sn_i and Se_i interstitials, etc., in $Cu_2ZnSnSe_4$ (similarly for Cu_2ZnSnS_4). They can be classified to be electron acceptors and donors according to the formal valences of the elements,[94] as shown in **Figure 5**. The formation energy change as a function of the Fermi energy is plotted in **Figure 6**, under the conditions of point P in the stable chemical potential region (Figure 3).

The most obvious trend in Figure 6 is that the formation energy of Cu_{Zn} antisite is lower than those of other defects, including V_{Cu}. According to Equation 3, the dependence of the formation energies on the chemical potentials is also plotted in **Figure 7** for the low-energy defects when the Fermi energy is near the VBM, which further confirms that Cu_{Zn} is always the dominant defect in the stable chemical potential region.

The dominance of the Cu_{Zn} antisite rather than V_{Cu} is one important feature in the defect properties of the kesterites Cu_2ZnSnS_4 and $Cu_2ZnSnSe_4$, at variance with the character in the defect properties of their parent compounds ($CuInSe_2$ or $CuGaSe_2$).[97–99] Comparing the formation energy of V_{Cu} in $Cu_2ZnSnSe_4$ with those in $CuInSe_2$ and $CuGaSe_2$, it can be found that the values at $\mu_{Cu} = 0$ are actually similar, about 0.8 eV. The ranges of μ_{Cu} that stabilize the three compounds are also similar (between –0.5 and 0 eV), so the formation energy of V_{Cu} in $Cu_2ZnSnSe_4$ is close to those in $CuInSe_2$ and $CuGaSe_2$. The formation energy of Cu_{Zn} is actually higher than that of V_{Cu} when $\mu_{Cu} = 0$ and $\mu_{Zn} = 0$, but the stable chemical potential range of μ_{Zn} is rather low (always lower than –1.2 eV, shown in Figure 3) as a result of the strong competition from ZnS, which decreases the formation energy of Cu_{Zn} by more than 1.2 eV and makes it more favorable than V_{Cu}.

Except for Cu_{Zn} and V_{Cu}, other acceptor defects such as V_{Zn}, Zn_{Sn} and Cu_{Sn} have much higher formation energy, no matter at what chemical potential in the stable region, as plotted in Figure 7. Therefore their contribution to the electrical conductivity should be negligible in the single-phase Cu_2ZnSnS_4 and $Cu_2ZnSnSe_4$ samples.

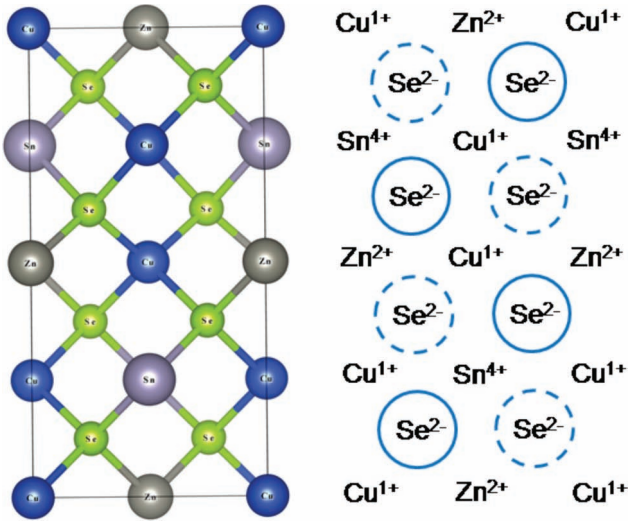

Figure 5. The crystal structure (left) and the nominal valence of cations and anions (right) of kesterite $Cu_2ZnSnSe_4$. The circles show that the Se anions are in the 8-electron full shell state (solid and dashed circles mean the Se anions are in different layers parallel to the plane).

On the side of donor defects, they all have high formation energy in the neutral state, much higher than those of the low-energy acceptors, as shown in Figure 6. This gives a clear explanation to the widely observed intrinsic p-type conductivity in Cu_2ZnSnS_4 and $Cu_2ZnSnSe_4$ samples.[8,20,34,37,55–64] Furthermore, intentional doping of Cu_2ZnSnS_4 and $Cu_2ZnSnSe_4$ to n-type through extrinsic elements may also be challenging, because the Cu_{Zn} and V_{Cu} acceptors can form spontaneously when the Fermi energy level is shifted up from near the VBM and compensate the introduced donors, as in $CuInSe_2$ and $CuGaSe_2$.[52]

Since kesterite samples naturally occur as p-type, and the Fermi energy is thus near the VBM, the donor defects can be ionized and decrease the formation energies of the charged

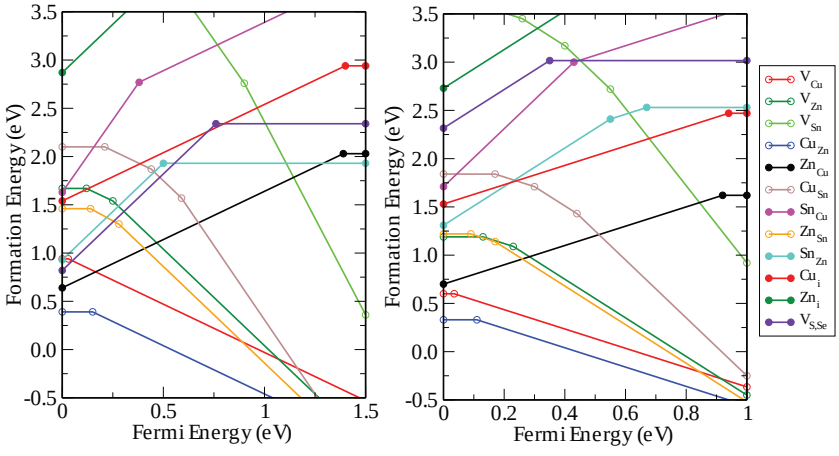

Figure 6. The change of the defect formation energy in Cu_2ZnSnS_4 (left) and $Cu_2ZnSnSe_4$ (right) as a function of the Fermi energy at the chemical potential point P (from Figure 3). For the same Fermi energy, only the most stable charge state is plotted, and the charge state changes at the circles (open for acceptors and filled for donors), which show the transition energy levels.

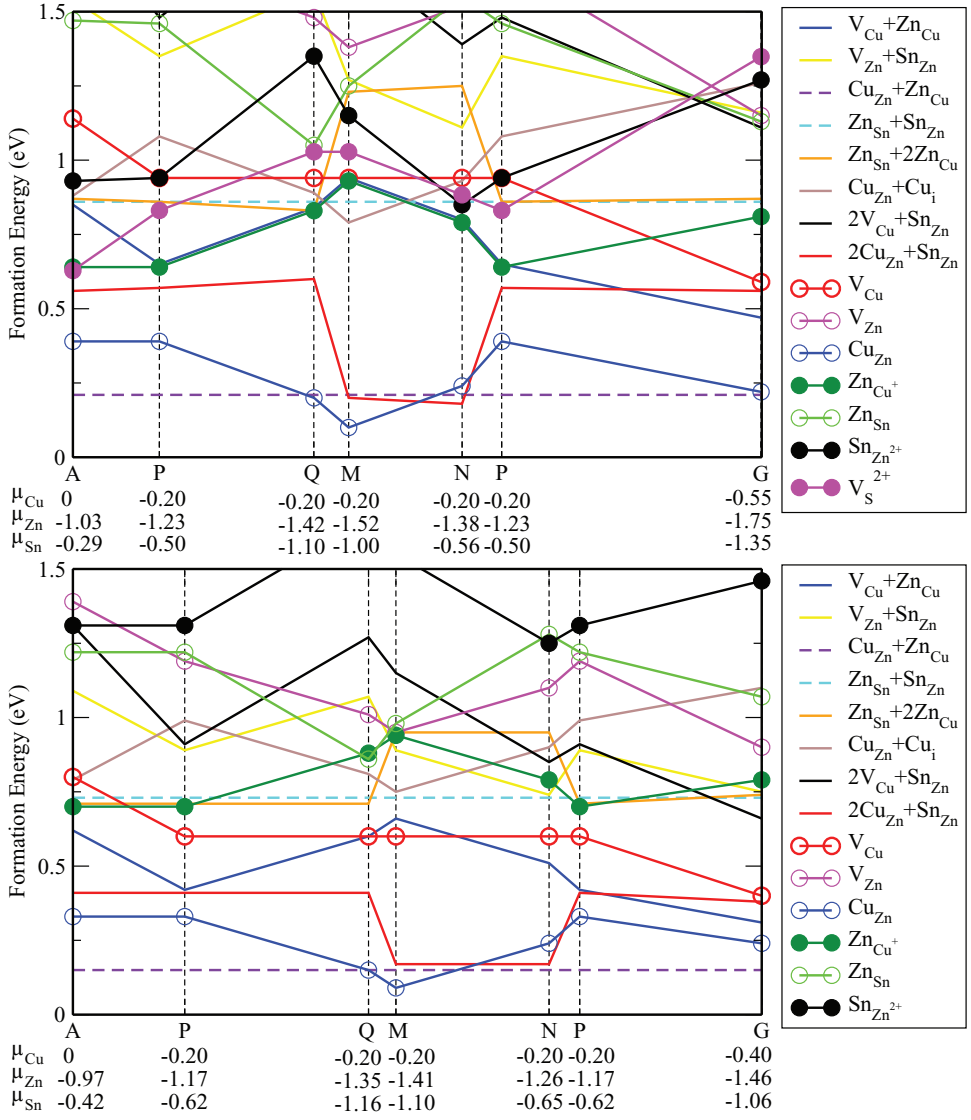

Figure 7. The formation energy of low-energy defects in Cu_2ZnSnS_4 (top) and $Cu_2ZnSnSe_4$ (bottom) as a function of the chemical potential along the APQMNPG lines surrounding the stable region shown in Figure 3. The Fermi energy is assumed at the top of the valence band (p-type conditions), and thus the donor defects are fully ionized.

states to low values, according to Equation 3. As plotted in Figure 6, the positively charged Zn_{Cu}^{+}, Sn_{Zn}^{2+} and V_S^{2+} have much lower formation energy than their neutral states when the Fermi energy is near the VBM. Under certain environments, their formation energies can be even lower than 0.75 eV, especially in Cu_2ZnSnS_4 as shown in Figure 7, which corresponds to a population on the order of 10^9 cm^{-3} at room temperature.

In the above discussion, the chemical potential is limited to the stable region, so the results are for the defects in nearly stoichiometric samples. When the chemical potential goes beyond the stable chemical potential region, i.e., the secondary or non-stoichiometric phases co-exist, the formation energies and population of different defects can be changed dramatically (according to Equation 3), so the dominant defects can be different too. For example, in the Cu_2ZnSnS_4 and $Cu_2ZnSnSe_4$ samples with Cu/(Zn+Sn) = 0.8 and Zn/Sn = 1.2 (which corresponds to the Cu poor and Zn rich condition frequently used in the experiments), the formation energies of V_{Cu} and Zn_{Sn} are decreased, while those of Cu_{Zn} and Sn_{Zn} are increased dramatically, making V_{Cu} the dominant acceptor. To show the population of different defects in these non-stoichiometric samples, a section detailing the defect and carrier concentration control is given later in the paper.

5.2. Transition Energy Levels

Whether the low-energy defects can produce free carriers and contribute to the electrical conductivity depends on their transition (ionization) levels, which can be derived according to the turning points in Figure 6 and are plotted in **Figure 8**.

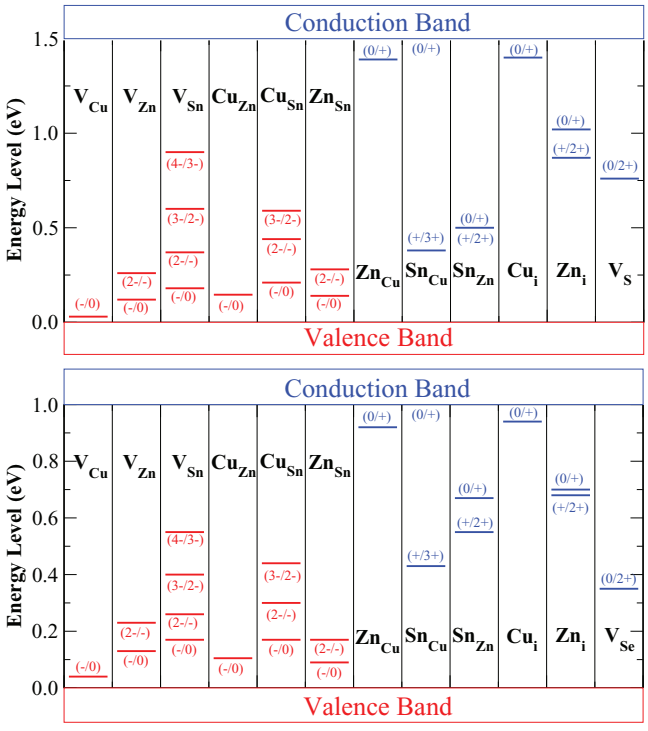

Figure 8. The ionization levels of intrinsic defects in the band gaps of Cu_2ZnSnS_4 (top) and $Cu_2ZnSnSe_4$ (bottom). The red bars show the acceptor levels and the blue bars show the donor levels, with the initial and final charge states labeled in parentheses. The calculated (using density functional theory) band gaps are corrected to the experimental values of 1.5 eV and 1.0 eV, respectively. Note that the new correction scheme (see Section 2.2) used in the current work gives deeper donor levels for Sn_{Cu}, Sn_{Zn} and Zn_i than previously reported results.[98]

Acceptor levels of V_{Cu} and Cu_{Zn}: As an intrinsic defect common to both Cu-based chalcopyrites and kesterites, the acceptor level introduced by V_{Cu} is always shallow. It is not affected by the replacement of the group III cations (Ga or In) by the group II (Zn) and IV (Sn) cations. The calculated (-/0) transition energy level of V_{Cu} (ionized from neutral to -1 charged) in $Cu_2ZnSnSe_4$ is similar to that in $CuGaSe_2$ and $CuInSe_2$, and the value in Cu_2ZnSnS_4 is even 10 meV shallower.

The (-/0) level of Cu_{Zn} is 0.11 eV in $Cu_2ZnSnSe_4$ and 0.15 eV in Cu_2ZnSnS_4 according to the present calculation (128-atom supercell), which are both deeper than the values of V_{Cu}. The deeper level of Cu_{Zn} is easy to understand according to the band component near the gap, as shown in **Figure 9**. Like the Cu-based chalcopyrites, kesterite Cu_2ZnSnS_4 and $Cu_2ZnSnSe_4$ have their upper valence band mainly composed of the antibonding states between Cu 3d and S 3p (or Se 4p). This hybridization is enhanced when one Zn atom is replaced by Cu, while weakened when one Cu is replaced by a vacancy, so the associated acceptor level of Cu_{Zn} is pushed up, and thus appears deeper than that of V_{Cu}. Within the same hybridization framework, we can also understand why the Cu_{Zn} level is slightly shallower (by 0.04 eV) in $Cu_2ZnSnSe_4$ than in Cu_2ZnSnS_4, considering the weaker hybridization in the selenide due to the longer Cu-Se bond. In Ref. [98], the wavefunction of the Cu_{Zn} acceptor level shows its distribution is mainly around Cu and S, similar to that of VBM. On the other hand, the delocalized distribution also confirms that the Cu_{Zn} acceptor state is not a deep localized state, and actually the absolute position of the level is not so deep; although it is deeper than that of V_{Cu}. The ionization of the dominant Cu_{Zn} antisites with a high population can produce a significant amount of hole carriers and result in good p-type conductivity, as discussed in the next section.

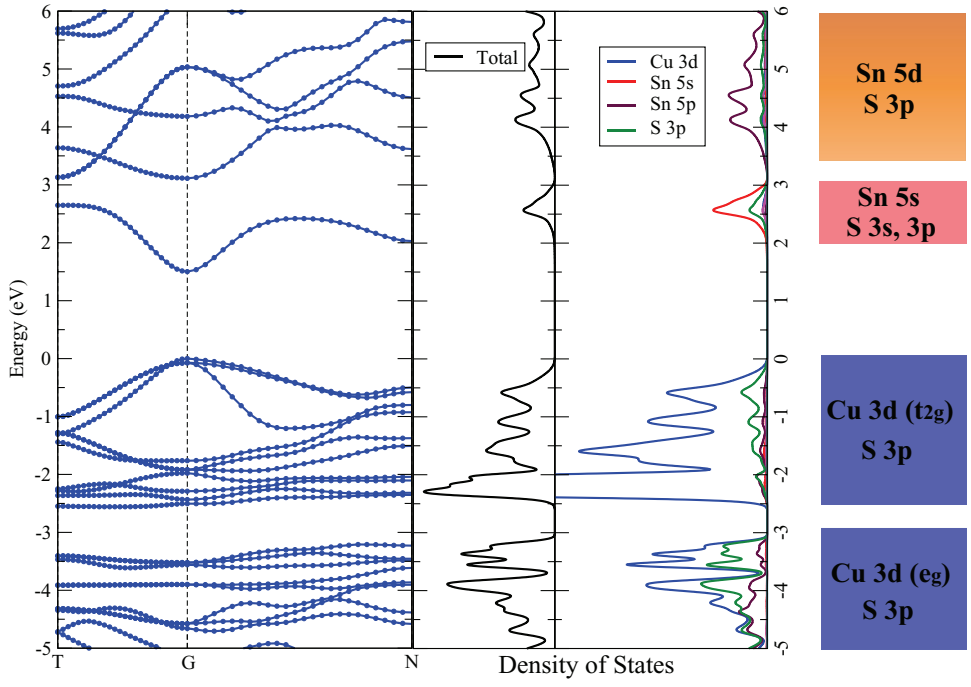

Figure 9. The calculated band structure, total and partial density of states, and the schematic plot of the band component for kesterite Cu_2ZnSnS_4. Here a hybrid exchange-correlation functional (HSE06) is used.[106,136,137]

Recently the experimental characterization of the acceptor levels has also been reported. Using admittance spectroscopy, Gunawan et al. observed a dominant acceptor with energy level of 0.13–0.2 eV in several high performance $Cu_2ZnSn(S,Se)_4$ solar cells with bandgap between 1.0 and 1.5 eV, consistent with the calculated Cu_{Zn} (-/0) levels in Cu_2ZnSnS_4 and $Cu_2ZnSnSe_4$. Fernandes et al. revealed two defect activation energies of 45 meV and 113 meV in Cu_2ZnSnS_4, which agree well with the calculated (-/0) levels of V_{Cu} and Cu_{Zn}, respectively.[88] Using capacitance spectroscopy, Barkhouse et al. observed a dominant defect level at 156 meV with an integrated defect density of 1.2×10^{15} cm^{-3} in the Cu poor and Zn rich $Cu_2ZnSn(S,Se)_4$ solar cell which has a efficiency as high as 10.1%.[22] This level can also be associated with the Cu_{Zn} defect considering the error in the calculations and experiments, and the order of the defect concentration is comparable with the Cu_{Zn} concentration when the Cu/(Zn+Sn) ratio is low, as discussed in the section 6.1.

All other acceptor defects (Cu_{Sn}, Zn_{Sn}, V_{Zn} and V_{Sn}) are high in formation energy (Figure 7), and induce a valence change of more than two. The acceptor levels associated with them, especially the transition between the high charge states such as (4-/3-) and (3-/2-), are deep. As a result, their contribution to the observed p-type conductivity could be negligible in the single-phase kesterite samples. However, they could contribute to luminescence and act as recombination centers.

Shallow donor level of Zn_{Cu}: Across the stable elemental chemical potential range, the charged Zn_{Cu}^{+} antisite is the lowest-energy donor when the sample is p-type. Its (0/+) transition energy level is shallow in both Cu_2ZnSnS_4 and $Cu_2ZnSnSe_4$, in contrast to the dominant donor Ga_{Cu}^{2+} in $CuGaSe_2$. The reason could be understood from two points: (i) Cu and Zn have small differences in both the size and the chemical valence, thus the replacement has small impact on the electronic structure; (ii) the conduction band is composed mainly of the Sn 5s and S 3s (Se 4s) states (see Figure 9), almost independent of Cu and Zn 4s states, which are much higher in energy than Sn 5s (see Table 2 of Ref. [24]). The electronic wavefunction of the Zn_{Cu} donor state resembles that of the CBM, mainly around Sn and S,[98] confirming the weak influence of the Zn_{Cu} antisite itself.

Deep donor levels: Since the kesterite Cu_2ZnSnS_4 and $Cu_2ZnSnSe_4$ are intrinsically p-type, the deep levels of the charged donor defects can act as electron-hole recombination centers, which could limit the performance of the kesterite solar cells. The deep donor levels in Cu_2ZnSnS_4 and $Cu_2ZnSnSe_4$ can be seen in Figure 8, e.g., those of Sn_{Cu}, Sn_{Zn}, Zn_i, V_S and V_{Se}.

The shallow Sn_{Cu} (0/+) level, and deep Sn_{Cu} (+/3+) and Sn_{Zn} (0/+) and (+/2+) levels can be explained according to the atomic orbital energies of Sn 5s and 5p states, as listed in Table 2 of Ref. [24]. When Sn replaces Cu, three extra electrons (two 5s electrons and one 5p electron) occupy the donor levels. As a result of the high orbital energy, the Sn 5p electron can be ionized easily, which makes Sn_{Cu} (0/+) extremely shallow and even in the conduction band according to the present calculation. However, as a result of the much lower 5s orbital energy, the ionization of the two 5s electrons is more difficult, and thus the (+/3+) level is deep in the band gap. Similarly when Sn replaces Zn, two 5s electrons occupy the donor levels and thus the (0/+) and (+/2+) levels are almost as deep as Sn_{Cu} (+/3+) level. The same mechanism also explains why Sn can be stable in compounds with both the upper 4+ and lower 2+ oxidation states,[119] and the so-called multi-valence of Sn.[100] Since the formation energy of Sn_{Cu} and Sn_{Zn} decreases when Sn becomes richer and Cu, Zn become poorer, they (especially the charged Sn_{Zn}^{2+} as shown in Figure 7) may have high population in samples with low Zn/Sn and Cu/Sn ratio, which could be detrimental to the solar cell performance.

The deep donor levels of anion vacancies (V_S and V_{Se}) have been reported in many chalcogenide semiconductors.[120,121] In $CuGaSe_2$ and $CuInSe_2$ the calculated levels of V_{Se} are both deep, but their formation energy (no matter in neutral or charged state) is quite high and thus their contribution can be neglected. A similar situation exists for V_{Se} in $Cu_2ZnSnSe_4$. However, the positively charged V_S^{2+} in Cu_2ZnSnS_4 has a formation energy as low as 0.8 eV in the p-type samples, so a significant amount of deep V_S donor levels may exist in Cu_2ZnSnS_4 when the cation/anion ratio is higher than unity. This suggests that sufficient sulfurization could be important for improving Cu_2ZnSnS_4 solar cell performance. Comparing the formation energies of the two deep donor defects (the charged Sn_{Zn} antisite and anion vacancies) in Cu_2ZnSnS_4 and $Cu_2ZnSnSe_4$, we found that they could be lower than 1.0 eV in Cu_2ZnSnS_4, while they are much higher in $Cu_2ZnSnSe_4$ (see Figure 7). This could be a reason for why the efficiencies of $Cu_2ZnSnSe_4$ or $Cu_2ZnSn(S,Se)_4$ alloy solar cells have been higher than those of the Cu_2ZnSnS_4 cells (see Table 1).

5.3. Donor-Acceptor Compensation

Donor-acceptor compensation in the ternary materials $CuGaSe_2$ and $CuInSe_2$ ($[2V_{Cu}^{-}+Ga_{Cu}^{2+}]$ and $[2V_{Cu}^{-}+In_{Cu}^{2+}]$, respectively) are well known to have electrically benign character even in highly non-stoichiometric samples. Whether the same behavior exists in the quaternary kesterites is an important question. Considering the multitude of low-energy intrinsic defects in the quaternary compounds (see Figure 6), various self-compensated defect clusters can be formed, such as $[Cu_{Zn}^{-}+Zn_{Cu}^{+}]$, $[Zn_{Sn}^{2-}+Sn_{Zn}^{2+}]$, $[V_{Cu}^{-}+Zn_{Cu}^{+}]$, $[2V_{Cu}^{-}+Sn_{Zn}^{2+}]$, $[2Cu_{Zn}^{-}+Sn_{Zn}^{2+}]$ and $[Zn_{Sn}^{2-}+2Zn_{Cu}^{+}]$. The calculation shows clearly that the overall formation energies of these defect clusters are significantly decreased relative to the sum of isolated ones. Electron transfer occurs from donor to acceptor defects and there is a strong Coulomb attraction between the charge centers, as explained previously. The clusters that have an overall formation energy lower than 1.5 eV are given in Figure 7 and their energy dependence on the chemical potentials is plotted.

Cation exchange and partial-disorder: Cu_{Zn} and Zn_{Cu} are the lowest-energy acceptor and donor defects, respectively, in both Cu_2ZnSnS_4 and $Cu_2ZnSnSe_4$. Their compensation leads to the antisite pair $[Cu_{Zn}^{-}+Zn_{Cu}^{+}]$ (in the following the labels of charge state will be omitted for brevity as $[Cu_{Zn}+Zn_{Cu}]$), which has an extremely low formation energy of 0.2 eV. When these antisite pairs interact with each other and arrange in a specific orientation (such as the (001) plane[24,106]), the average formation energy can be further decreased. A high population can be expected, which results in the partially disorder of Cu and Zn on the cation sites along (001) planes. Due to the similarity of Cu and Zn in the atomic number and size, the Cu and Zn

partial disorder can not be detected easily using standard XRD techniques, which makes the kesterite structure sometimes confused as the stannite structure.[55,89] The existence of the partial disorder in Cu_2ZnSnS_4 and $Cu_2ZnSnSe_4$ have been confirmed using the neutron scattering method by the group of Schorr.[122,123]

Although there may be a high population of $[Cu_{Zn}+Zn_{Cu}]$ in the samples, their impact on the electronic structure and optical properties is weak, as shown by the slight band edge shift caused by a pair in the 128-atom supercell (see **Figure 10**), and thus they can be taken as benign defects. However, two other antisite pairs $[Cu_{Sn}+Sn_{Cu}]$ and $[Zn_{Sn}+Sn_{Zn}]$ are not so benign and have more significant impact on the electronic structure, e.g., $[Zn_{Sn}+Sn_{Zn}]$ decreases the band gap by 0.3 eV in Cu_2ZnSnS_4 and 0.1 eV in $Cu_2ZnSnSe_4$. Fortunately their formation energy is high and the resulting population should be negligible (see Figure 7).

As the antisite pairs are stoichiometry-preserving defects, their formation energies and population are independent of the element chemical potentials or the Cu/(Zn+Sn) and Zn/Sn ratios.

Defect clusters causing non-stoichiometry: The aforementioned antisite pairs are stoichiometric, so the frequently observed non-stoichiometry in Cu_2ZnSnS_4 and $Cu_2ZnSnSe_4$ samples must come from other sources. Some defect clusters like $[V_{Cu}+Zn_{Cu}]$, $[V_{Zn}+Sn_{Zn}]$, $[Zn_{Sn}+2Zn_{Cu}]$ and $[2Cu_{Zn}+Sn_{Zn}]$ exchange atoms with the environment, so their formation energies are more sensitive to the chemical potential of the component elements (the Cu/(Zn+Sn) and Zn/Sn ratios) than those of isolated defects (see Equation 3). Such defects could be the primary source of non-stoichiometry.

For the majority of the chemical potential range that stabilizes single-phase Cu_2ZnSnS_4 and $Cu_2ZnSnSe_4$, $[2Cu_{Zn}+Sn_{Zn}]$ clusters have the lowest formation energies, about 0.2–0.6 eV depending on the specific chemical potentials, as shown in Figure 7. This corresponds to a population range from about 10^{11} to 10^{18} cm^{-3}. Although a population of 10^{18} cm^{-3} clusters causes a change in the Cu/(Zn+Sn) and Zn/Sn ratios of around 0.0001, which is beyond the current limit of most analysis techniques, their influence on the generation, separation and recombination of electron-hole pairs can be significant. It is thus important to investigate the effects of $[2Cu_{Zn}+Sn_{Zn}]$ defect clusters in the nominally stoichiometric single-phase samples.[124]

Another low-energy defect cluster in the stable chemical potential range is $[V_{Cu}+Zn_{Cu}]$, whose formation energy can be as low as 0.4 and 0.3 eV in Cu_2ZnSnS_4 and $Cu_2ZnSnSe_4$,

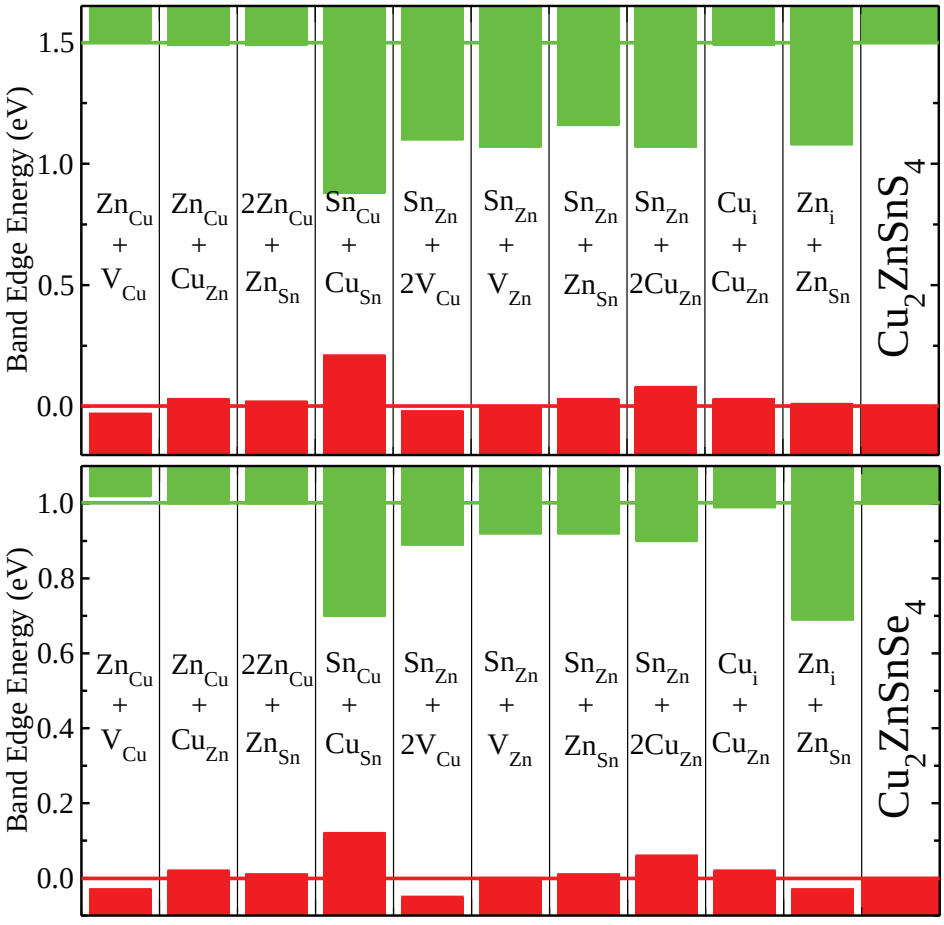

Figure 10. The calculated valence and conduction band shifts caused by different defect clusters in Cu_2ZnSnS_4 (top panel) and $Cu_2ZnSnSe_4$ (bottom panel). The defect concentration is one defect cluster in an 128-atom supercell. The red and green lines show the valence and conduction band positions, respectively.

respectively. All other clusters have higher formation energy in the stable chemical potential space, but the values can be changed significantly when the chemical potential goes beyond the boundaries.

According to the calculated formation energy in Figure 7 and the numbers of exchanged atoms in the formation of different clusters, the contributing defects to the non-stoichiometric element ratios can be predicted. [V_{Cu}+Zn_{Cu}] and [Zn_{Sn}+2Zn_{Cu}] should be the highest-population defects and contribute to the low Cu/(Zn+Sn) and high Zn/Sn ratios when Cu and Sn are poor (very negative μ_{Cu} and μ_{Sn}), whereas [2Cu_{Zn}+Sn_{Zn}] should be the highest-population defects and contribute to the high Cu/(Zn+Sn) and low Zn/Sn ratio when Zn is poor (very negative μ_{Zn}). More quantitative predictions will be discussed in the next section.

Bandedge shifts: Compared to the perfect bulk semiconductor, the conduction and valence band edges of the material with high concentrations of defect clusters are shifted in energy. These fluctuations in potential will impact electron and hole transport. Figure 10 plots the band edge shift for ten possible self-compensated defect clusters when the defect concentration is equal to one defect cluster in an 128-atom supercell. Because of the hybridization between the donor and acceptor states, the conduction band edge in Figure 10 is higher than the corresponding donor level in Figure 8, and the valence band edge is lower than the corresponding acceptor level. For example, the hybridization between Cu_{Zn} acceptor and Zn_{Cu} donor states make the band edge shift caused by [Cu_{Zn}+Zn_{Cu}] cluster small, and the resulting band gap decrease is negligible. The band gap is even locally increased by [V_{Cu}+Zn_{Cu}] due to the valence band downshift.

More significant shifts are associated with defect clusters composed of the deep level defects, such as Sn_{Zn}, Sn_{Cu}, Cu_{Sn} and Zn_i. The conduction band edge downshift induced by all clusters composed of Sn_{Zn} is similar, about 0.4 eV in Cu_2ZnSnS_4 and 0.1 eV in $Cu_2ZnSnSe_4$. The quite large downshift caused by Sn_{Zn} related clusters in Cu_2ZnSnS_4 could be a detrimental factor to the solar cell performance if their population is high, because the induced states are deep and may trap photo-generated electrons from the high conduction band. Considering that the population of [2Cu_{Zn}+Sn_{Zn}] clusters could be as high as 10^{18} cm^{-3} even in the chemical potential conditions that stabilize the single-phase Cu_2ZnSnS_4 (Cu/(Zn+Sn) and Zn/Sn ratios near 1), the solar cell performance could be limited by these clusters and special treatment may be required to prevent their formation.

Impact on the photovoltaic performance: The frequently mentioned experimental observation that a low Cu/(Zn+Sn) ratio around 0.8 and a high Zn/Sn ratio around 1.2 (Cu poor and Zn rich) gives the highest solar cell efficiencies,[1,3,5,6,15,25–29] as shown in Figure 1 and Table 1, can be explained partly according to the detrimental effect of [2Cu_{Zn}+Sn_{Zn}] clusters. The formation energy of [2Cu_{Zn}+Sn_{Zn}] is very sensitive to the chemical potential of Zn, so when Zn becomes poor, its population increases dramatically and degrades the solar cell performance. However, low Cu/(Zn+Sn) and high Zn/Sn ratio mean that Zn is very rich during the growth environment, which is just the condition preventing the formation of [2Cu_{Zn}+Sn_{Zn}] clusters, so the resultant higher efficiency is easy to understand. Although a low Cu/(Zn+Sn) ratio near 0.8 and a high Zn/Sn ratio near 1.2 also mean the sample is seriously non-stoichiometric, the contributing defect clusters are benign ones such as [V_{Cu}+Zn_{Cu}] and [Zn_{Sn}+2Zn_{Cu}] that induce almost negligible band edge shifts. Besides the low population of detrimental [2Cu_{Zn}+Sn_{Zn}] clusters, three factors are beneficial to the solar cell efficiency under Zn rich and Cu poor conditions:

(i) a high population of [V_{Cu}+Zn_{Cu}] clusters are formed in some domains within the CZTS or CZTSe absorber layers, resulting in band bending that can facilitate the separation of photo-generated electron-hole pairs[97,98];
(ii) the shallow acceptor V_{Cu} becomes the dominant defect, in place of the relatively deeper Cu_{Zn}, and determines the population of the majority carriers (holes);
(iii) the population of isolated defects with deep donor levels is diminished, such as Sn_{Zn}^{2+}, which has a formation energy lower than 1.0 eV in Cu_2ZnSnS_4 (Figure 6) and acts as a recombination center.

Comparing the defect properties in Cu_2ZnSnS_4 and $Cu_2ZnSnSe_4$, we can also explain another empirical trend drawn from the numbers in Table 1 that the $Cu_2ZnSnSe_4$ and $Cu_2ZnSn(S,Se)_4$ solar cells have higher record efficiencies than the Cu_2ZnSnS_4 solar cells. It can result from two differences:

(i) the conduction band edge downshift caused by [2Cu_{Zn}+Sn_{Zn}] in $Cu_2ZnSnSe_4$ is much smaller than in Cu_2ZnSnS_4 (0.4 eV), so the electron trapping effect is much weaker in $Cu_2ZnSnSe_4$;
(ii) the formation energies of the isolated deep donor defects Sn_{Zn}^{2+} and V_{Se}^{2+} are much higher in $Cu_2ZnSnSe_4$ than in Cu_2ZnSnS_4, so the concentration of the recombination centers is lower.

The nominal band gap of Cu_2ZnSnS_4 is larger than that of $Cu_2ZnSnSe_4$, but the photo-generated electrons may be trapped on the deep defect levels, which can limit the open-circuit voltage and the efficiency to a low value. As listed in Table 1, currently the highest open-circuit voltage of pure Cu_2ZnSnS_4 solar cells is about 0.66 eV, close to the value (about 0.71 eV) of the highest-efficiency $Cu(In,Ga)Se_2$ cells, while lower than that (about 0.85 eV) of CdTe cells.[125] Considering that the band gaps of Cu_2ZnSnS_4, $Cu(In,Ga)Se_2$ (when the efficiency is highest) and CdTe are in the order 1.5, 1.2 and 1.5 eV, the open-circuit voltage of the current Cu_2ZnSnS_4 cells is lower than expected.

These differences may impose a limitation on the efficiency and the open-circuit voltage of $Cu_2ZnSn(S,Se)_4$ solar cells. The band gap of $Cu_2ZnSn(S,Se)_4$ alloys can be increased linearly from 1.0 eV to 1.5 eV through increasing the S content,[126] closer to the optimal band gap (1.5 eV) for single-junction solar cell absorber, so the efficiency is expected to be improved. However, the record efficiency has been achieved for $Cu_2ZnSn(S,Se)_4$ alloys with low S content.[1,6,12,23,82] Recently Barkhouse et al. even observed that the efficiencies of the alloy cells with band gaps lower than 1.2 eV are higher than those with band gaps larger than 1.4 eV.[71] This is similar to the situation in $Cu(In,Ga)Se_2$ solar cells that the efficiency can be increased through alloying a low content of Ga, but further increasing the band gap above 1.2 eV causes an efficiency decrease.

6. Defect and Carrier Concentration Control

All of the above discussion on the defect populations and electrical conductivity is qualitative. We will quantify defect and carrier concentration in the samples with different Cu/(Zn+Sn) and Zn/Sn ratios. Since the formation energy and transition energy levels of many defects are calculated, and the lattice parameters, electronic band gaps and effective masses have also been reported,[127] it is possible to calculate the concentration of these defects and the majority carriers in the samples under different chemical potential conditions, through self-consistently determining the Fermi energy.[105] The calculated Cu, Zn and Sn element ratios, population (density) of different defects, Fermi energy and the concentration (density) of the majority carrier (hole) at room temperature are plotted as functions of the chemical potentials μ_{Cu}, μ_{Zn} and μ_{Sn} in **Figure 11**.

6.1. Cu Composition Control

The defect and hole concentration change in Cu_2ZnSnS_4 and $Cu_2ZnSnSe_4$ when the Cu chemical potential varies from poor to rich (μ_{Cu} increases from –0.52 to 0 eV) is shown in Figure 11 (a) and (d). The vertical lines show the chemical potential point P, which is in the region stabilizing the single-phase quaternary compound (Figure 3). Starting from the single-phase and stoichiometric line, the concentrations of the dominant acceptor Cu_{Zn} and Cu_{Zn}^- increase exponentially when μ_{Cu} increases, which results in a lower Fermi energy, higher hole concentration and better p-type conductivity. However, the concentration of the detrimental [$2Cu_{Zn}$+Sn_{Zn}] defect clusters also increases exponentially, which degrades the solar cell performance despite the good p-type conductivity.

On the other side of the vertical line, when μ_{Cu} decreases, the concentrations of both Cu_{Zn} and Cu_{Zn}^- and thus the hole concentration decrease, but when μ_{Cu} is lower than a certain value (–0.4 eV for Cu_2ZnSnS_4 and –0.3 eV for $Cu_2ZnSnSe_4$), the concentration of another acceptor (V_{Cu} and V_{Cu}^-) increases, which make the hole concentration increase after reaching a minimum point, so the p-type conductivity is enhanced when Cu becomes poorer and V_{Cu} becomes more dominant than Cu_{Zn}. Meanwhile, when Cu becomes poor, the concentration of the [V_{Cu}+Zn_{Cu}] and [Zn_{Sn}+$2Zn_{Cu}$] defect clusters increases exponentially, which causes serious non-stoichiometry, i.e., the Cu and Zn element ratio deviating from the ideal values (2 and 1 respectively in the stoichiometric case). Fortunately these two defect clusters have little influence on the electronic structure of the kesterites (Figure 10) and are electrically benign, so their high population has no negative affect on the solar cell performance. Actually, the valence band downshift caused by [V_{Cu}+Zn_{Cu}] clusters is even beneficial to the performance since they enhance the electron-hole separation in the light-absorber layer.

The above discussion gives a more quantitative explanation to why a low Cu/(Zn+Sn) ratio (around 0.8) or a Cu poor and Zn rich condition is crucial to the high efficiency of the kesterite solar cells. Under those conditions, the population of the detrimental [$2Cu_{Zn}$+Sn_{Zn}] defect clusters is forced to be very low, while a reasonably high concentration (around 10^{15}– 10^{16} cm^{-3}) of holes from the ionized V_{Cu}^- is achieved. Experimentally, the measurement of the hole concentration in the high-efficiency Cu_2ZnSnS_4 and $Cu_2ZnSnSe_4$ solar cells shows that the values are around 5×10^{15} cm^{-3} when the Cu/(Zn+Sn) ratio is near 0.8,[22,65] in good agreement with the present calculation considering that both the experimental and theoretical methods can have relatively large margins of error. When the Cu/(Zn+Sn) ratio is high (around 1), various measurements show that the hole concentration is much higher with numbers scattered from 10^{17} to 10^{19} cm^{-3},[32,34,56,66,67,69,70] which can be attributed to the region near or on the right hand side of the vertical lines in Figure 11 (a) and (d). In this region, the concentrations of Cu_{Zn}^- and holes vary around 10^{16}–10^{18} cm^{-3} and the Cu/(Zn+Sn) ratio is around 1, both consistent with the measured results. However, the 10^{16}–10^{18} cm^{-3} population of [$2Cu_{Zn}$+Sn_{Zn}] will result in a poor photovoltaic performance. This gives an explanation to the reported low efficiency of Cu_2ZnSnS_4 solar cells with Cu/(Zn+Sn) around 1.[27,29,67,73,76,77]

6.2. Zn and Sn Composition Control

The defect and hole concentration changes as a function of μ_{Zn} and μ_{Sn} are plotted for Cu_2ZnSnS_4 in Figure 11 (b) and (c), respectively, and for $Cu_2ZnSnSe_4$ in Figure 11 (e) and (f), respectively.

Several trends can be drawn:

(i) Under the considered conditions, the holes come mainly from the ionization of the Cu_{Zn} antisites, so the hole population decreases exponentially with μ_{Zn} when Zn becomes rich (μ_{Cu} is fixed), while the change in μ_{Sn} (Sn richness) has weak influence on the hole concentration;

(ii) Three defect clusters [$2Cu_{Zn}$+Sn_{Zn}], [V_{Cu}+Zn_{Cu}] and [Zn_{Sn}+$2Zn_{Cu}$] contribute significantly to non-stoichiometry, i.e., when either Zn is very rich or Sn is very poor, the concentration of [Zn_{Sn}+$2Zn_{Cu}$] and [V_{Cu}+Zn_{Cu}] can be very high, e.g., higher than 10^{20} cm^{-3} when Zn/Sn ratio is around 1.05; while when either Zn is very poor or Sn is very rich, the concentration of [$2Cu_{Zn}$+Sn_{Zn}] becomes high.

From these trends and the numbers in Figure 11, the concentration of defects in the samples with different Cu/(Zn+Sn) and Zn/Sn ratios can be estimated, and thus their influence on the solar cell performance can be predicted. Meanwhile, it should be noticed that when the Cu, Zn and Sn element ratios are obviously deviated from ideal values due to the high population of defect clusters (Figure 11), their chemical potentials are actually far from the stable chemical potential range of Cu_2ZnSnS_4 and $Cu_2ZnSnSe_4$, so the real samples are not single-phase microscopically and the secondary compounds should coexist, e.g., when Cu/(Zn+Sn) = 0.8 and Zn/Sn = 1.2, ZnS or ZnSe formation should be expected.[42,47,49]

7. Conclusions

The increased number of elements in the quaternary kesterite materials makes the properties of the intrinsic lattice defects

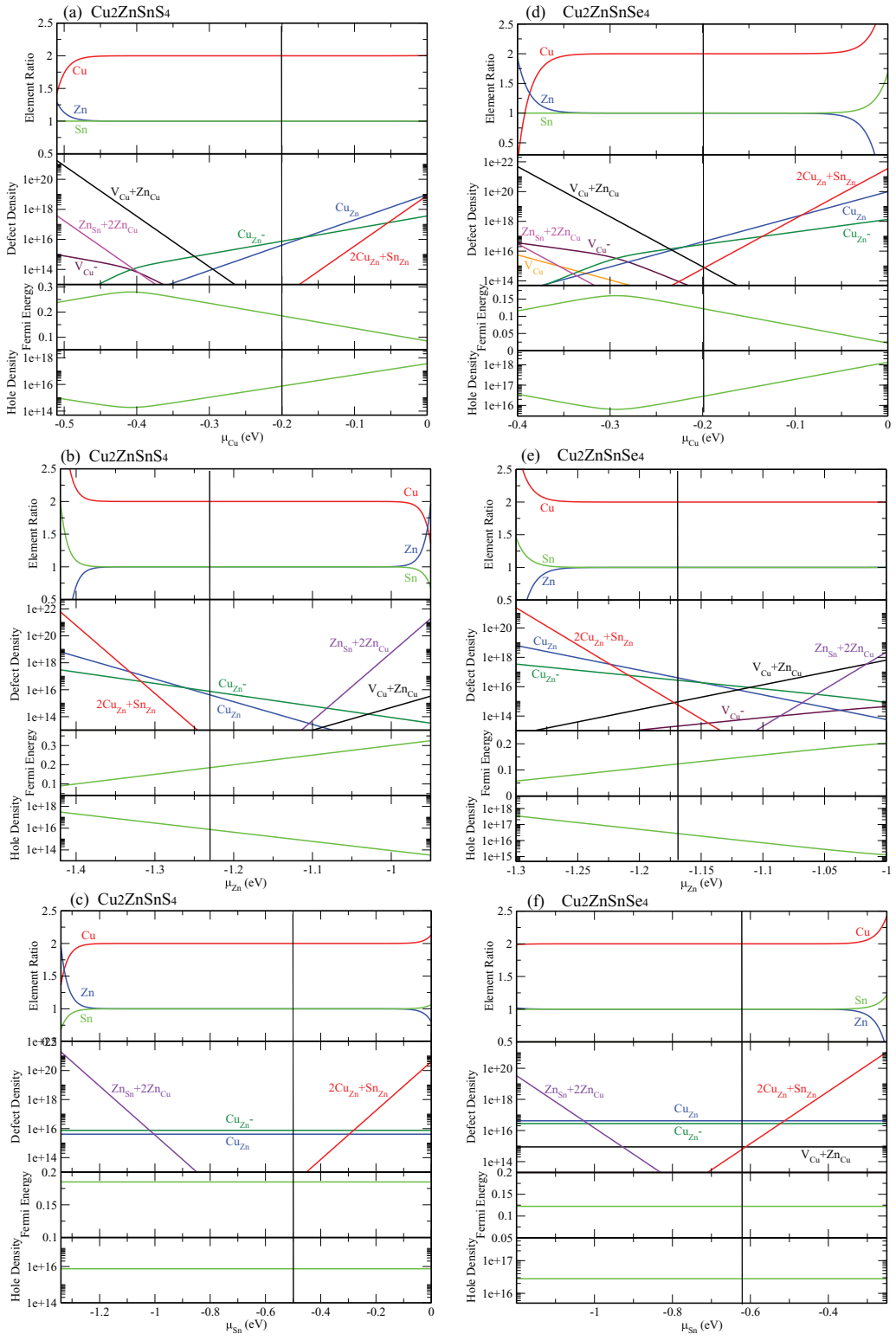

Figure 11. The calculated change of the element ratio, defect density (cm^{-3}), Fermi energy (in eV relative to the valence band) and hole density (cm^{-3}) at room temperature for Cu_2ZnSnS_4 (left column): (a) μ_{Cu} changes from –0.52 to 0 eV, with μ_{Zn} = –1.23 eV and μ_{Sn} = –0.50 eV; (b) μ_{Zn} changes from –1.53 to –0.93 eV, with μ_{Cu} = –0.20 eV and μ_{Sn} = –0.50 eV; (c) μ_{Sn} changes from –1.35 to 0 eV, with μ_{Cu} = –0.20 eV and μ_{Zn} = –1.23 eV; and $Cu_2ZnSnSe_4$ (right column): (d) μ_{Cu} changes from –0.4 to 0 eV, with μ_{Zn} = –1.17 eV and μ_{Sn} = –0.62 eV; (e) μ_{Zn} changes from –1.3 to –1.0 eV, with μ_{Cu} = -0.20 eV and μ_{Sn} = –0.62 eV; (f) μ_{Sn} changes from –1.2 to –0.25 eV, with μ_{Cu} = –0.20 eV and μ_{Zn} = –1.17 eV. The vertical lines in the figure show the chemical potential corresponding to the point P in Figure 3.

Table 2. Comparison of the band gap, electrical conductivity and intrinsic defects in the chalcopyrites and kesterites.

	$CuInSe_2$	$CuGaSe_2$	$Cu_2ZnSnSe_4$	Cu_2ZnSnS_4
Band gap (eV)	1.04	1.68	1.0	1.5
Intrinsic conductivity	p-type	p-type	p-type	p-type
Hole-generating acceptors	V_{Cu}^-	V_{Cu}^-	Cu_{Zn}^-, V_{Cu}^-	Cu_{Zn}^-, V_{Cu}^-
High-population deep donors		Ga_{Cu}^{2+}		Sn_{Zn}^{2+}, V_S^{2+}
High-population clusters	$2V_{Cu}+In_{Cu}$	$2V_{Cu}+Ga_{Cu}$	$V_{Cu}+Zn_{Cu}$	$V_{Cu}+Zn_{Cu}$
			$Cu_{Zn}+Zn_{Cu}$	$Cu_{Zn}+Zn_{Cu}$
			$2Cu_{Zn}+Sn_{Zn}$	$2Cu_{Zn}+Sn_{Zn}$
			$Zn_{Sn}+2Zn_{Cu}$	$Zn_{Sn}+2Zn_{Cu}$
Electron trapping clusters		$2V_{Cu}+Ga_{Cu}$		$2Cu_{Zn}+Sn_{Zn}$

more complicated than for the previously studied ternary chalcopyrites. They are also more important in influencing the photovoltaic performance. Several points can be highlighted:

(1) The narrow chemical potential range is limited by the various competing secondary compounds, such as CuS, Cu_2S, Cu_2SnS_3, ZnS, SnS and SnS_2. ZnS and ZnSe coexistence is highly possible in the kesterites with low Cu/(Zn+Sn) and high Zn/Sn ratios.

(2) The Cu_{Zn} antisite is the dominant point defect in the stoichiometric Cu_2ZnSnS_4 and $Cu_2ZnSnSe_4$ samples. Its ionization level is deeper than that of V_{Cu}, but its high population can still produce a significant hole concentration, determining the intrinsic p-type conductivity and making n-type doping difficult.

(3) The formation energy and ionization level of V_{Cu} in kesterites are similar to those in the chalcopyrites, but the population is much lower than Cu_{Zn} in the stoichiometric samples. Under Cu poor and Zn rich conditions (Cu/(Zn+Sn) ≈ 0.8), V_{Cu} becomes dominant and contributes to p-type conductivity, which reflects the situation in the real solar cells with low Cu/(Zn+Sn) ratio and high efficiency.

(4) The frequently observed non-stoichiometry in the quaternary kesterites results from the facile formation of self-compensated defect clusters, such as $[V_{Cu}+Zn_{Cu}]$, $[Zn_{Sn}+2Zn_{Cu}]$ and $[2Cu_{Zn}+Sn_{Zn}]$.

(5) $[2Cu_{Zn}+Sn_{Zn}]$ clusters induce electron-trapping states in the absorber materials, and are thus detrimental to the solar cell performance. Their facile formation and high population even in the near-stoichiometric Cu_2ZnSnS_4 and $Cu_2ZnSnSe_4$ samples degrades the efficiency of the solar cells with Cu/(Zn+Sn) and Zn/Sn ratios near unity, so a rather Zn rich and Cu, Sn poor condition is required to prevent its formation and improve the solar cell performance. This explains the empirical observation that Cu poor and Zn rich condition is crucial for the high solar cell efficiency.

(6) The electron-trapping caused by $[2Cu_{Zn}+Sn_{Zn}]$ in $Cu_2ZnSnSe_4$ is much weaker than in Cu_2ZnSnS_4, is the main reason for the observation that the $Cu_2ZnSn(S,Se)_4$ solar cells achieve the highest-efficiency when S composition is low. The lower population of isolated deep donor defects such as Sn_{Zn} and V_{Se} in $Cu_2ZnSnSe_4$ is another reason. Considering the negative effects of lattice defects in Cu_2ZnSnS_4, a limitation for the solar cell efficiency and the open-circuit voltage of $Cu_2ZnSn(S,Se)_4$ solar cells exists, similar to $Cu(In,Ga)Se_2$, where the highest efficiency is achieved at relatively low Ga composition.

Finally, a comparison of the defect properties in the four chalcopyrites and kesterites is given in **Table 2** based on the calculated results. The present study concerning the fundamental defect properties in Cu_2ZnSnS_4 and $Cu_2ZnSnSe_4$ is useful not only for their application as the solar cell absorber, but also for the study of other kesterite or stannite structured I_2-II-IV-VI_4 semiconductors which may have application as thermoelectric, photocatalytic and optoelectronic materials.[54,128–135]

Acknowledgements

The work in China is supported by National Natural Science Foundation (No. 61106087, 10934002 and 91233121), the Special Funds for Major State Basic Research (No. 2012CB921401), the Research Program of Shanghai municipality and MOE, PCSIRT and CC of ECNU. A.W. acknowledges support from the Royal Society for a University Research Fellowship and EPSRC Grant No. EP/I01330X/1. The work at NREL is funded by the US Department of Energy, under Contract No. DE-AC36-08GO28308.

Received: August 1, 2012
Revised: October 15, 2012
Published online: February 11, 2013

[1] a) T. K. Todorov, K. B. Reuter, D. B. Mitzi, *Adv. Mater.* **2010**, *22*, E156; b) D. B. Mitzi, O. Gunawan, T. K. Todorov, K. Wang, S. Guha, *Sol. Energy Mater. Sol. Cells* **2011**, *95*, 1421.
[2] A. Walsh, S. Chen, S.-H. Wei, X. G. Gong, *Adv. Energy Mater.* **2012**, *2*, 400.
[3] H. Katagiri, K. Jimbo, W. S. Maw, K. Oishi, M. Yamazaki, H. Araki, A. Takeuchi, *Thin Solid Films* **2009**, *517*, 2455.
[4] S. Siebentritt, S. Schorr, *Prog. Photovolt.: Res. Appl.* **2012**, *20*, 512.
[5] H. Wang, *Int. J. Photoenergy* **2011**, *2011*, 801292.
[6] W. Ki, H. W. Hillhouse, *Adv. Energy Mater.* **2011**, *1*, 732.
[7] S. Ahn, S. Jung, J. Gwak, A. Cho, K. Shin, K. Yoon, D. Park, H. Cheong, J. H. Yun, *Appl. Phys. Lett.* **2010**, *97*, 021905.
[8] M. Grossberg, J. Krustok, K. Timmo, M. Altosaar, *Thin Solid Films* **2009**, *517*, 2489.
[9] S. G. Choi, H. Y. Zhao, C. Persson, C. L. Perkins, A. L. Donohue, B. To, A. G. Norman, J. Li, I. L. Repins, *J. Appl. Phys.* **2012**, *111*, 033506.

[10] F. Luckert, D. I. Hamilton, M. V. Yakushev, N. S. Beattie, G. Zoppi, M. Moynihan, I. Forbes, A. V. Karotki, A. V. Mudryi, M. Grossberg, J. Krustok, R. W. Martin, *Appl. Phys. Lett.* **2011**, *99*, 062104.
[11] D. Park, D. Nam, S. Jung, S. An, J. Gwak, K. Yoon, J. H. Yun, H. Cheong, *Thin Solid Films* **2011**, *519*, 7386.
[12] K. Timmo, M. Altosaar, J. Raudoja, K. Muska, M. Pilvet, M. Kauk, T. Varema, M. Danilson, O. Volobujeva, E. Mellikov, *Sol. Energy Mater. Sol. Cells* **2010**, *94*, 1889.
[13] M. Grossberg, J. Krustok, J. Raudoja, K. Timmo, M. Altosaar, T. Raadik, *Thin Solid Films* **2011**, *519*, 7403.
[14] W. Shockley, H. J. Queisser, *J. Appl. Phys.* **1961**, *32*, 510.
[15] I. Repins, C. Beall, N. Vora, C. DeHart, D. Kuciauskas, P. Dippo, B. To, J. Mann, W.-C. Hsu, A. Goodrich, R. Noufi, *Sol. Energy Mater. Sol. Cells* **2012**, *101*, 154.
[16] C. H. L. Goodman, *J. Phys. Chem. Solids* **1958**, *6*, 305.
[17] B. R. Pamplin, *J. Phys. Chem. Solids* **1964**, *25*, 675.
[18] K. Ito, T. Nakazawa, *Jpn. J. Appl. Phys.* **1988**, *27*, 2094.
[19] T. M. Friedlmeier, N. Wieser, T. Walter, H. Dittrich, H. W. Schock, *Proceedings of the 14th European PVSEC*, Barcelona, Spain, page 1242, **1997**.
[20] H. Katagiri, K. Saitoh, T. Washio, H. Shinohara, T. Kurumadani, S. Miyajima, *Sol. Energy Mater. Sol. Cells* **2001**, *65*, 141.
[21] T. K. Todorov, J. Tang, S. Bag, O. Gunawan, T. Gokmen, Y. Zhu, D. B. Mitzi, *Adv. Energy Mater.* **2013**, *3*, 34.
[22] D. Barkhouse, O. Gunawan, T. Gokmen, T. Todorov, D. Mitzi, *Prog. Photovolt.: Res. Appl.* **2012**, *20*, 6.
[23] S. Bag, O. Gunawan, T. Gokmen, Y. Zhu, T. K. Todorov, D. B. Mitzi, *Energy Environ. Sci.* **2012**, *5*, 7060.
[24] S. Chen, X. G. Gong, A. Walsh, S.-H. Wei, *Phys. Rev. B* **2009**, *79*, 165211.
[25] H. Katagiri, K. Jimbo, M. Tahara, H. Araki, K. Oishi, *Mater. Res. Soc. Symp. Proc.* **2009**, *1165*, 1165-M04-01.
[26] K. Tanaka, M. Oonuki, N. Moritake, H. Uchiki, *Sol. Energy Mater. Sol. Cells* **2009**, *93*, 583.
[27] A. Ennaoui, M. Lux-Steiner, A. Weber, D. Abou-Ras, I. Koetschau, H. W. Schock, R. Schurr, A. Hoelzing, S. Jost, R. Hock, T. Voß, J. Schulze, A. Kirbs, *Thin Solid Films* **2009**, *517*, 2511.
[28] B. Shin, O. Gunawan, Y. Zhu, N. A. Bojarczuk, S. J. Chey, S. Guha, *Prog. Photovolt.: Res. Appl.* **2011**, DOI: 10.1002/pip.1174.
[29] K. Tanaka, Y. Fukui, N. Moritake, H. Uchiki, *Sol. Energy Mater. Sol. Cells* **2011**, *95*, 838.
[30] F. Hergert, R. Hock, *Thin Solid Films* **2007**, *515*, 5953.
[31] P. Salomé, J. Malaquias, P. Fernandes, M. Ferreira, J. Leitao, A. da Cunha, J. González, F. Matinaga, G. Ribeiro, E. Viana, *Sol. Energy Mater. Sol. Cells* **2011**, *95*, 3482.
[32] S. W. Shin, S. Pawar, C. Y. Park, J. H. Yun, J.-H. Moon, J. H. Kim, J. Y. Lee, *Sol. Energy Mater. Sol. Cells* **2011**, *95*, 3202.
[33] A. Wangperawong, J. King, S. Herron, B. Tran, K. Pangan-Okimoto, S. Bent, *Thin Solid Films* **2011**, *519*, 2488.
[34] R. A. Wibowo, W. S. Kim, E. S. Lee, B. Munir, K. H. Kim, *J. Phys. Chem. Solids* **2007**, *68*, 1908.
[35] H. Katagiri, *Thin Solid Films* **2005**, *480–481*, 426.
[36] K. Sekiguchi, K. Tanaka, K. Moriya, H. Uchiki, *Phys. Status Solidi c* **2006**, *3*, 2618.
[37] X. Zhang, X. Shi, W. Ye, C. Ma, C. Wang, *Appl. Phys. A - Mater. Sci. Processing* **2009**, *94*, 381.
[38] T. Todorov, M. Kita, J. Carda, P. Escribano, *Thin Solid Films* **2009**, *517*, 2541.
[39] J. Scragg, P. Dale, L. Peter, *Thin Solid Films* **2009**, *517*, 2481.
[40] R. Schurr, A. Hoelzing, S. Jost, R. Hock, T. Voss, J. Schulze, A. Kirbs, A. Ennaoui, M. Lux-Steiner, A. Weber, I. Kötschau, H.-W. Schock, *Thin Solid Films* **2009**, *517*, 2465.
[41] T. Tanaka, T. Sueishi, K. Saito, Q. Guo, M. Nishio, K. M. Yu, W. Walukiewicz, *J. Appl. Phys.* **2012**, *111*, 053522.
[42] G. S. Babu, Y. K. Kumar, P. U. Bhaskar, S. R. Vanjari, *Sol. Energy Mater. Sol. Cells* **2010**, *94*, 221.
[43] J. T. Watjen, J. Engman, M. Edoff, C. Platzer-Bjorkman, *Appl. Phys. Lett.* **2012**, *100*, 173510.
[44] Y.-T. Zhai, S. Chen, J.-H. Yang, H.-J. Xiang, X.-G. Gong, A. Walsh, J. Kang, S.-H. Wei, *Phys. Rev. B* **2011**, *84*, 075213.
[45] K. Wang, B. Shin, K. B. Reuter, T. Todorov, D. B. Mitzi, S. Guha, *Appl. Phys. Lett.* **2011**, *98*, 051912.
[46] X. Fontane, L. Calvo-Barrio, V. Izquierdo-Roca, E. Saucedo, A. Perez-Rodriguez, J. R. Morante, D. M. Berg, P. J. Dale, S. Siebentritt, *Appl. Phys. Lett.* **2011**, *98*, 181905.
[47] A. Redinger, K. Hoenes, X. Fontane, V. Izquierdo-Roca, E. Saucedo, N. Valle, A. Perez-Rodriguez, S. Siebentritt, *Appl. Phys. Lett.* **2011**, *98*, 101907.
[48] P. Fernandes, P. Salomé, A. da Cunha, *J. Alloys Compd.* **2011**, *509*, 7600.
[49] J. Just, D. Luetzenkirchen-Hecht, R. Frahm, S. Schorr, T. Unold, *Appl. Phys. Lett.* **2011**, *99*, 262105.
[50] J. T. Waetjen, J. Engman, M. Edoff, C. Platzer-Bjoerkman, *Appl. Phys. Lett.* **2012**, *100*, 173510.
[51] S. B. Zhang, S.-H. Wei, A. Zunger, H. Katayama-Yoshida, *Phys. Rev. B* **1998**, *57*, 9642.
[52] C. Persson, Y.-J. Zhao, S. Lany, A. Zunger, *Phys. Rev. B* **2005**, *72*, 035211.
[53] C. D. R. Ludwig, T. Gruhn, C. Felser, J. Windeln, *Phys. Rev. B* **2011**, *83*, 174112.
[54] S. Levcenko, N. Syrbu, E. Arushanov, V. Tezlevan, R. Fernandez-Ruiz, J. Merino, M. Leon, *J. Appl. Phys.* **2006**, *99*, 073513.
[55] N. Nakayama, K. Ito, *Appl. Surf. Sci.* **1996**, *92*, 171.
[56] T. Tanaka, T. Nagatomo, D. Kawasaki, M. Nishio, Q. Guo, A. Wakahara, A. Yoshida, H. Ogawa, *J. Phys. Chem. Solids* **2005**, *66*, 1978.
[57] J. J. Scragg, P. J. Dale, L. M. Peter, G. Zoppi, I. Forbes, *Phys. Status Solidi b* **2008**, *245*, 1772.
[58] M. Altosaar, J. Raudoja, K. Timmo, M. Danilson, M. Grossberg, J. Krustok, E. Mellikov, *Phys. Status Solidi a* **2008**, *205*, 167.
[59] K. Oishi, G. Saito, K. Ebina, M. Nagahashi, K. Jimbo, W. S. Maw, H. Katagiri, M. Yamazaki, H. Araki, A. Takeuchi, *Thin Solid Films* **2008**, *517*, 1449.
[60] Y. K. Kumar, G. S. Babu, P. U. Bhaskar, V. S. Raja, *Sol. Energy Mater. Sol. Cells* **2009**, *93*, 1230.
[61] K. Hones, E. Zscherpel, J. Scragg, S. Siebentritt, *Physica B: Condensed Matter* **2009**, *404*, 4949.
[62] N. Shinde, D. Dubal, D. Dhawale, C. Lokhande, J. Kim, J. Moon, *Mater. Res. Bull.* **2012**, *47*, 302.
[63] Y. Miyamoto, K. Tanaka, M. Oonuki, N. Moritake, H. Uchiki, *Jpn. J. Appl. Phys.* **2008**, *47*, 596.
[64] T. Prabhakar, N. Jampana, *Sol. Energy Mater. Sol. Cells* **2011**, *95*, 1001.
[65] K. Wang, O. Gunawan, T. Todorov, B. Shin, S. J. Chey, N. A. Bojarczuk, D. Mitzi, S. Guha, *Appl. Phys. Lett.* **2010**, *97*, 143508.
[66] J. P. Leitão, N. M. Santos, P. A. Fernandes, P. M. P. Salomé, A. F. da Cunha, J. C. González, G. M. Ribeiro, F. M. Matinaga, *Phys. Rev. B* **2011**, *84*, 024120.
[67] Z. Zhou, Y. Wang, D. Xu, Y. Zhang, *Sol. Energy Mater. Sol. Cells* **2010**, *94*, 2042.
[68] C. Chan, H. Lam, C. Surya, *Sol. Energy Mater. Sol. Cells* **2010**, *94*, 207.
[69] J. Zhang, L. Shao, Y. Fu, E. Xie, *Rare Metals* **2006**, *25*, 315.
[70] R. A. Wibowo, E. S. Lee, W. S. Kim, B. Munir, K. H. Kim, *Phys. Status Solidi a* **2007**, *204*, 3373.
[71] D. W. Miller, C. W. Warren, O. Gunawan, T. Gokmen, D. B. Mitzi, J. D. Cohen, *Appl. Phys. Lett.* **2012**, *101*, 142106.

[72] H. Katagiri, K. Jimbo, S. Yamada, T. Kamimura, W. S. Maw, T. Fukano, T. Ito, T. Motohiro, *Appl. Phys. Express* **2008**, *1*, 041201.
[73] S. C. Riha, B. A. Parkinson, A. L. Prieto, *J. Am. Chem. Soc.* **2009**, *131*, 12054.
[74] N. Moritake, Y. Fukui, M. Oonuki, K. Tanaka, H. Uchiki, *Phys. Status Solidi c* **2009**, *6*, 1233.
[75] K. Moriya, K. Tanaka, H. Uchiki, *Jpn. J. Appl. Phys.* **2007**, *46*, 5780.
[76] K. Maeda, K. Tanaka, Y. Fukui, H. Uchiki, *Sol. Energy Mater. Sol. Cells* **2011**, *95*, 2855.
[77] H. Araki, Y. Kubo, K. Jimbo, W. S. Maw, H. Katagiri, M. Yamazaki, K. Oishi, A. Takeuchi, *Phys. Status Solidi c* **2009**, *6*, 1266.
[78] B.-A. Schubert, B. Marsen, S. Cinque, T. Unold, R. Klenk, S. Schorr, H.-W. Schock, *Prog. Photovolt.: Res. Appl.* **2011**, *19*, 93.
[79] R. Chalapathy, G. S. Jung, B. T. Ahn, *Sol. Energy Mater. Sol. Cells* **2011**, *95*, 3216.
[80] A. R. Jeong, W. Jo, S. Jung, J. Gwak, J. H. Yun, *Appl. Phys. Lett.* **2011**, *99*, 082103.
[81] G. Zoppi, I. Forbes, R. W. Miles, P. J. Dale, J. J. Scragg, L. M. Peter, *Prog. Photovolt: Res. Appl.* **2009**, *17*, 315.
[82] Q. Guo, G. M. Ford, W.-C. Yang, B. C. Walker, E. A. Stach, H. W. Hillhouse, R. Agrawal, *J. Am. Chem. Soc.* **2010**, *132*, 17384.
[83] A. Redinger, D. M. Berg, P. J. Dale, S. Siebentritt, *J. Am. Chem. Soc.* **2011**, *133*, 3320.
[84] T. Todorov, O. Gunawan, S. J. Chey, T. G. de Monsabert, A. Prabhakar, D. B. Mitzi, *Thin Solid Films* **2011**, *519*, 7378.
[85] K. Tanaka, Y. Miyamoto, H. Uchiki, K. Nakazawa, H. Araki, *phys. stat. sol. a* **2006**, *203*, 2891.
[86] M. J. Romero, H. Du, G. Teeter, Y. Yan, M. M. Al-Jassim, *Phys. Rev. B* **2011**, *84*, 165324.
[87] O. Gunawan, T. Gokmen, C. W. Warren, J. D. Cohen, T. K. Todorov, D. A. R. Barkhouse, S. Bag, J. Tang, B. Shin, D. B. Mitzi, *Appl. Phys. Lett.* **2012**, *100*, 253905.
[88] P. A. Fernandes, A. F. Sartori, P. M. P. Salomé, J. Malaquias, A. F. da Cunha, M. P. F. Graça, J. C. González, *Appl. Phys. Lett.* **2012**, *100*, 233504.
[89] A. Shavel, J. Arbiol, C. Andreu, *J. Am. Chem. Soc.* **2010**, *132*, 4514.
[90] S. C. Riha, B. A. Parkinson, A. L. Prieto, *J. Am. Chem. Soc.* **2011**, *133*, 15272.
[91] G. M. Ford, Q. Guo, R. Agrawal, H. W. Hillhouse, *Chem. Mater.* **2011**, *23*, 2626.
[92] J. Wang, X. Xin, Z. Lin, *Nanoscale* **2011**, *3*, 3040.
[93] J.-J. Wang, J.-S. Hu, Y.-G. Guo, L.-J. Wan, *NPG Asia Mater.* **2012**, *4*, e2.
[94] S.-H. Wei, *Comp. Mater. Sci.* **2004**, *30*, 337.
[95] C. G. Van de Walle, J. Neugebauer, *J. Appl. Phys.* **2004**, *95*, 3851.
[96] S. B. Zhang, J. E. Northrup, *Phys. Rev. Lett.* **1991**, *67*, 2339.
[97] S. Chen, X. G. Gong, A. Walsh, S.-H. Wei, *Appl. Phys. Lett.* **2010**, *96*, 021902.
[98] S. Chen, J.-H. Yang, X. G. Gong, A. Walsh, S.-H. Wei, *Phys. Rev. B* **2010**, *81*, 245204.
[99] A. Nagoya, R. Asahi, R. Wahl, G. Kresse, *Phys. Rev. B* **2010**, *81*, 113202.
[100] K. Biswas, S. Lany, A. Zunger, *Appl. Phys. Lett.* **2010**, *96*, 201902.
[101] T. Maeda, S. Nakamura, T. Wada, *Thin Solid Films* **2011**, *519*, 7513.
[102] J. M. Raulot, C. Domain, J. F. Guillemoles, *J. Phys. Chem. Solids* **2005**, *66*, 2019.
[103] S. Lany, A. Zunger, *Phys. Rev. Lett.* **2008**, *100*, 016401.
[104] S. Sze, *Physics of Semiconductor Devices*, 2nd ed. Wiley, New York, **1981**.
[105] J. Ma, S.-H. Wei, T. A. Gessert, K. K. Chin, *Phys. Rev. B* **2011**, *83*, 245207.
[106] S. Chen, X. G. Gong, A. Walsh, S.-H. Wei, *Appl. Phys. Lett.* **2009**, *94*, 041903.
[107] W. Haas, T. Rath, A. Pein, J. Rattenberger, G. Trimmel, F. Hofer, *Chem. Commun.* **2011**, *47*, 2050.
[108] A. Weber, R. Mainz, H. W. Schock, *J. Appl. Phys.* **2010**, *107*, 013516.
[109] S.-H. Wei, S. B. Zhang, *J. Phys. Chem. Solids* **2005**, *66*, 1994.
[110] A. Zunger, S. Zhang, S.-H. Wei, *Conference Record of the Twenty-Sixth IEEE Photovoltaic Specialists Conference*, page 313 **1997**.
[111] S. Schuler, S. Siebentritt, S. Nishiwaki, N. Rega, J. Beckmann, S. Brehme, M. C. Lux-Steiner, *Phys. Rev. B* **2004**, *69*, 045210.
[112] C. L. Bailey, L. Liborio, G. Mallia, S. Tomi , N. M. Harrison, *Phys. Rev. B* **2010**, *81*, 205214.
[113] J. Pohl, T. Unold, K. Albe, arXiv:1205.2556v1, **2012**.
[114] J. Pohl, K. Albe, *J. Appl. Phys* **2010**, *108*, 023509.
[115] M. A. Contreras, K. Ramanathan, J. AbuShama, F. Hasoon, D. L. Young, B. Egaas, R. Noufi, *Prog. Photovolt: Res. Appl.* **2005**, *13*, 209.
[116] C. Persson, A. Zunger, *Appl. Phys. Lett.* **2005**, *87*, 211904.
[117] S. B. Zhang, S.-H. Wei, *Phys. Rev. B* **2002**, *65*, 081402.
[118] C.-S. Jiang, R. Noufi, J. A. AbuShama, K. Ramanathan, J. R. Moutinho, J. Pankow, M. M. Al-Jassim, *Appl. Phys. Lett.* **2004**, *84*, 3477.
[119] A. Walsh, G. W. Watson, *Phys. Rev. B* **2004**, *70*, 235114.
[120] S. Lany, A. Zunger, *Phys. Rev. B* **2005**, *72*, 035215.
[121] Y. Shirakawa, H. Kukimoto, *Solid State Commun.* **1980**, *34*, 359.
[122] S. Schorr, H. J. Hoebler, M. Tovar, *Eur. J. Mineral.* **2007**, *19*, 65.
[123] S. Schorr, *Sol. Energy Mater. Sol. Cells* **2011**, *95*, 1482.
[124] S. Chen, L.-W. Wang, A. Walsh, X.-G. Gong, S.-H. Wei, *Appl. Phys. Lett.* **2012**, *101*, 223901.
[125] M. A. Green, K. Emery, Y. Hishikawa, W. Warta, E. D. Dunlop, *Prog. Photovolt.: Res. Appl.* **2012**, *20*, 12.
[126] S. Chen, A. Walsh, J.-H. Yang, X. G. Gong, L. Sun, P.-X. Yang, J.-H. Chu, S.-H. Wei, *Phys. Rev. B* **2011**, *83*, 125201.
[127] C. Perrson, *J. Appl. Phys.* **2010**, *107*, 053710.
[128] M.-L. Liu, I.-W. Chen, F.-Q. Huang, L.-D. Chen, *Adv. Mater.* **2009**, *21*, 3808.
[129] C. Sevik, T. Çağin, *Phys. Rev. B* **2010**, *82*, 045202.
[130] C. Sevik, T. Çağin, *Appl. Phys. Lett.* **2009**, *95*, 112105.
[131] T. Arai, S. Tajima, S. Sato, K. Uemura, T. Morikawa, T. Kajino, *Chem. Commun.* **2011**, *47*, 12664.
[132] S. Ikeda, T. Nakamura, T. Harada, M. Matsumura, *Phys. Chem. Chem. Phys.* **2010**, *12*, 13943.
[133] I. Tsuji, Y. Shimodaira, H. Kato, H. Kobayashi, A. Kudo, *Chem. Mater.* **2010**, *22*, 1402.
[134] M. Leon, S. Levcenko, R. Serna, G. Gurieva, A. Nateprov, J. M. Merino, E. J. Friedrich, U. Fillat, S. Schorr, E. Arushanov, *J. Appl. Phys.* **2010**, *108*, 093502.
[135] X. Xin, M. He, W. Han, J. Jung, Z. Lin, *Angew. Chem.* **2011**, *50*, 11739.
[136] J. Paier, R. Asahi, A. Nagoya, G. Kresse, *Phys. Rev. B* **2009**, *79*, 115126.
[137] S. Botti, D. Kammerlander, M. A. L. Marques, *Appl. Phys. Lett.* **2011**, *98*, 241915.